Neutron Resonance Spectroscopy

Frank Gunsing

CEA/Saclay
DSM/DAPNIA/SPhN
F-91191 Gif-sur-Yvette

Mémoire d'Habilitation à Diriger des Recherches
présenté à l'Université Paris 7

Soutenu le 1er juin 2005
devant un jury composé de

Hubert Doubre, IN2P3/CSNSM
Bernard Haas, IN2P3/CENBG
Gérard Rudolf, IN2P3/IRES
Philippe Schwemling, IN2P3/LPNHE, Université Paris 7
Claude Stéphan, IN2P3/IPNO

Contents

Résumé 3

Summary 5

Introduction 7

1 Neutron data for science and technology 13

1.1 Parity nonconservation 13

1.2 Stellar nucleosynthesis 17

1.2.1 Stellar evolution 17

1.2.2 The s-process 19

1.2.3 The Maxwellian-averaged neutron capture cross section . . 21

1.3 Nuclear data for nuclear energy 24

1.3.1 Nuclear waste transmutation 25

1.3.2 The thorium cycle 27

1.4 Neutron data libraries 30

1.5 Statistical model observations 32

1.5.1 Partial width fluctuations 32

1.5.2 Level spacings 33

1.6 Neutron cross section measurements 35

1.6.1 Experimental facilities 35

1.6.2 The neutron time-of-flight method 36
1.6.3 Experimental considerations 36

2 The *R*-matrix formalism **39**
2.1 Introduction 39
2.2 Channel representation 41
2.3 The wave function in the external region 43
2.4 The collision matrix U 43
2.5 The relation between the cross sections and the collision matrix U . 45
2.6 The wave function in the internal region 46
2.6.1 Surface functions 46
2.6.2 Internal wave functions 47
2.7 The relation between the *R*-matrix and the collision matrix U 48
2.8 Approximations of the *R*-matrix 50
2.8.1 The Breit-Wigner Single Level approximation 51
2.8.2 The Breit-Wigner multi level approximation 52
2.8.3 The Reich-Moore approximation 52
2.9 Average cross sections 53

Conclusion **55**

References **56**

Annex **65**

Résumé

Le présent document a été écrit dans le but d'obtenir le diplôme "Habilitation à Diriger des Recherches". Comme ce diplôme est indispensable pour encadrer des étudiants préparant une thèse, j'ai voulu faire un document qui peut être utile pour quelqu'un qui débute dans la discipline de la spectroscopie des résonances neutroniques. Bien que les sujets traités dans ce document soient déjà décrits autre part, et souvent de façon plus détaillée, il m'a semblé utile de réunir ici la plupart de l'information appropriée.

Une introduction générale place la thématique de l'interaction neutron-noyau dans un contexte de physique nucléaire. Les grandes variations de plusieurs ordres de grandeurs dans les sections efficaces des réactions induites par neutrons sont expliquées en termes d'excitations des niveaux nucléaires. Le caractère aléatoire de ces résonances rend des prédictions par modèles nucléaires impossibles.

Ensuite, plusieurs domaines de physique où les réactions induites par neutrons sont importantes, et auxquels j'ai contribué d'une façon ou d'une autre, sont évoqués dans un premier chapitre de manière synthétique. Il s'agit de sujets tels que la non-conservation de la parité dans certaines résonances neutroniques, la nucléosynthèse stellaire par capture neutronique, et les données pour des applications de l'énergie nucléaire. Ce dernier thème est d'actualité en ce qui concerne la transmutation des déchets nucléaires et des cycles alternatifs du combustible. Les bibliothèques nucléaires sont aussi brièvement abordées.

Un deuxième chapitre traite en détail de la théorie de la matrice R. Ce formalisme est le fondement de la description de l'interaction neutron-noyau et revient dans tous les domaines de la spectroscopie des résonances neutroniques.

Summary

The present document has been written in order to obtain the diploma "Habilitation à Diriger des Recherches". Since this diploma is indispensable to supervise thesis students, I had the intention to write a document that can be useful for someone starting in the field of neutron resonance spectroscopy. Although the here described topics are already described elsewhere, and often in more detail, it seemed useful to have most of the relevant information in a single document.

A general introduction places the topic of neutron-nucleus interaction in a nuclear physics context. The large variations of several orders of magnitude in neutron-induced reaction cross sections are explained in terms of nuclear level excitations. The random character of the resonances make nuclear model calculation predictions impossible.

Then several fields in physics where neutron-induced reactions are important and to which I have contributed in some way or another, are mentioned in a first synthetic chapter. They concern topics like parity nonconservation in certain neutron resonances, stellar nucleosynthesis by neutron capture, and data for nuclear energy applications. The latter item is especially important for the transmutation of nuclear waste and for alternative fuel cycles. Nuclear data libraries are also briefly mentioned.

A second chapter details the *R*-matrix theory. This formalism is the foundation of the description of the neutron-nucleus interaction and is present in all fields of neutron resonance spectroscopy.

Introduction

One of the most striking features of neutron-nucleus interactions is the resonance structure observed in the reaction cross sections at low incident neutron energies. Since the electrically neutral neutron has no Coulomb barrier to overcome, and has a negligible interaction with the electrons in matter, it can directly penetrate and interact with the atomic nucleus, even at very low kinetic energies in the order of electron-volts.

The cross sections can show variations of several orders of magnitude on an energy scale of only a few eV. The origin of the resonances is well understood: they are related to the excitation of nuclear states in the compound nuclear system formed by the neutron and the target nucleus, at excitation energies lying above the neutron binding energy of typically several MeV.

The compound nucleus model was introduced by Niels Bohr to explain the observed resonances in neutron-nucleus reactions. The wavelength of low energy neutrons is comparable to the size of the nucleus. Typical widths Γ of measured resonances are in the order of electron-volts. According to Heisenberg's uncertainty principle, the corresponding life time of the compound nucleus is in the order of $\tau = \hbar/\Gamma \simeq 10^{-15}$ s, several orders of magnitude larger than the typical time needed by a neutron to cross a nucleus without interaction. In this picture, the neutron binding energy which becomes available to the compound nucleus, is rearranged among all nucleons, and gives rise to a complex configuration corresponding to a well defined nuclear state with an energy, spin and parity. Within Fermi's description of excitations of particle-hole configurations, such a state would correspond to an extremely complicated configuration of a many particle, many hole state. The compound nucleus may then decay through the energetically allowed channels. The way of decay and the decay probability of the compound nucleus is considered to be independent from the way how the compound nucleus was formed, but respecting conservation of energy and angular momentum. The decay probability is equal to the branching ratio Γ_x/Γ where Γ_x is the width related to the decay by emission of a particle x, which at low energy is mainly a gamma ray or a neutron.

In direct reactions, as the opposite reaction mechanism to compound nucleus reactions, the incident neutron interacts directly with one or a few nucleons without forming a compound nucleus. The time scale of direct reactions is in the order of 10^{-22} s and much shorter than compound-nucleus resonance reactions. Direct re-

actions become important for the heavier nuclei at neutron energies higher than about 10 MeV where the De Broglie wavelength of the neutron becomes comparable to the size of nucleons. But also at lower neutron energies, mainly for light A or closed shell nuclei, direct reactions may contribute significantly to the total reaction cross section. In general for neutrons with energies below 1 MeV the here discussed compound nucleus reactions prevail.

In figure 1 a picture of the compound nucleus reaction is sketched. After the formation of the highly excited state by an incident neutron, the compound nucleus can decay by emission of gamma radiation, which is called radiative neutron capture, or by by emission of a neutron, which is elastic scattering. If the kinetic energy of the neutron is high enough, threshold reactions are possible, like inelastic scattering, leaving the target nucleus in an excited state. If the excitation energy is higher than the fission threshold, fission is energetically allowed. Due to the pairing effect, the neutron binding energy for even compound nuclei is considerably lower than for odd compound nuclei, which for some of the heavy nuclei results in a fissionable nucleus even if the incident neutron has nearly zero kinetic energy. All these reactions show resonances at the same energies corre-

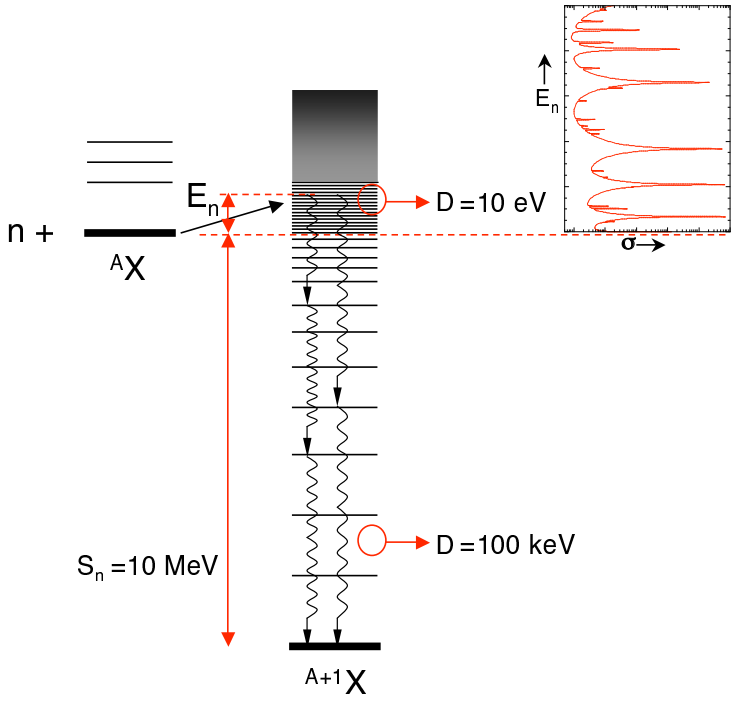

Figure 1: Schematic view of the formation and decay of a compound nucleus with typical values of level spacing and neutron separation energy. The resonances observed in the reaction cross section correspond to the excitation of nuclear levels.

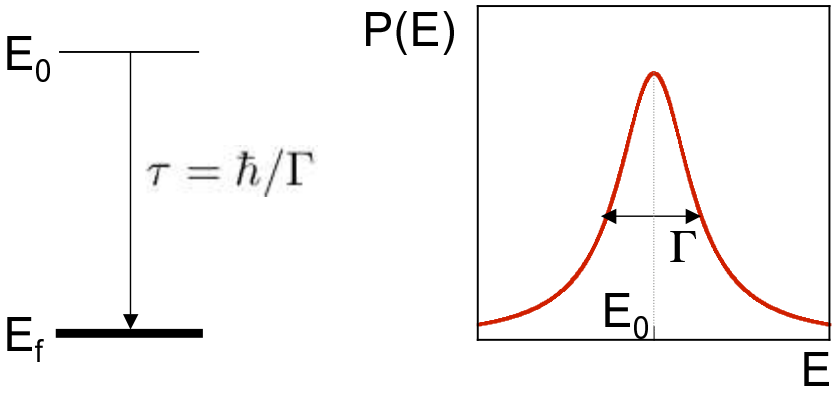

Figure 2: The Breit-Wigner shape of the energy profile (right) of a quantum state with a finite life time τ (left).

sponding to the excitation of the nuclear levels in the compound nucleus. The shapes of the resonances are different and related to the involved widths.

The possible neutron-nucleus reactions vary with incident neutron energy. The nuclear reaction that is always present if a reaction is energetically allowed is elastic scattering. This may be scattering from the nuclear potential, also called shape elastic or sometimes hard sphere scattering, without forming a compound nucleus. In addition resonant elastic scattering through a compound nucleus may be present. The potential scattering is a smooth and nearly energy independent cross section as a function of energy but interferes with the resonant scattering cross section.

The widths of isolated resonances in reaction cross sections have in good approximation a familiar Breit-Wigner shape. The time dependence of the wave function $\Psi(t)$ of a non-stationary state at E_0 with a life time $\tau = \hbar/\Gamma$, is observed as an exponential decay in time. The squared absolute value of the Fourier transform of $\Psi(t)$ gives the energy distribution $P(E)$ having the Breit-Wigner form

$$P(E) = \frac{\Gamma/2\pi}{(E - E_0)^2 + \Gamma^2/4} \tag{1}$$

which is the typical shape for any quantum-mechanical state with a finite lifetime. This equivalence in the time and energy domain is illustrated in figure 2.

In the limiting case of a single, isolated $\ell = 0$ resonance at low energy E_0 and with capture, fission and elastic scattering as the only open channels, the total cross section can be expressed in the single level Breit-Wigner form as

$$\sigma_T(E) = 4\pi R'^2 + \pi \lambda\!\!\!^{-2} g \left(\frac{4\Gamma_n (E - E_0) R'/\lambda\!\!\!^{-} + \Gamma_n^2 + \Gamma_n \Gamma_\gamma + \Gamma_n \Gamma_f}{(E - E_0)^2 + (\Gamma_n + \Gamma_\gamma + \Gamma_f +)^2/4} \right) \qquad (2)$$

where Γ_n is the neutron width, Γ_γ the radiative width, Γ_f the fission width, g the statistical spin factor and $\lambda\!\!\!^{-}$ the reduced de Broglie wave length of the neutron. The first term in the sum is the potential scattering cross section $\sigma_p = 4\pi R'^2$, where R' is the effective nuclear radius, with a value close to the channel radius a. the Full R-matrix expressions for the cross sections are given later.

At the high excitation energies above the neutron binding energies, for most nuclei the nuclear system is extremely complex and no nuclear model is capable of predicting the position and other properties of these excited states. Cross sections can therefore be accessed only by measurements. For a heavy nucleus the wave function describing such a highly excited state may have as much as 10^6 components. Also the level density in this region is consequently very high. A neighbouring eigenstate can be excited by only a small change in excitation energy and may have a completely different wave function. This is a manifestation of what is also called chaotic behaviour. Due to extreme configuration mixing, the nucleus in this regime above the neutron threshold has a statistical behaviour. This is expressed by the assumption that the matrix elements relating nuclear states have a random character, governed by a Gaussian distribution with zero mean. This statistical model of the compound nucleus is referred to as the Gaussian Orthogonal Ensemble (GOE) [1–5].

The statistical model has direct consequences on the observables of the reaction cross sections. The channel widths are proportional to the square of the matrix elements and have therefore a chi-squared distribution with one degree of freedom. also called the Porter-Thomas distribution [6]. The observed gamma width of a resonance is the sum of many, for medium and heavy nuclei several tens of thousand, individual gamma widths and tends therefore more to a Gaussian distribution. Observed fission widths correspond to a relatively small number of fission channels, at maximum three or four. The resulting distribution can be approximated by an effective chi-squared distribution with a small, fractional number of degrees of freedom [7].

With increasing excitation energy the widths of the states start to overlap and the resulting cross sections become smooth. The properties of the eigenstates, like the decay widths, fluctuating from one state to another, become apparent as values averaged over many resonances. These average values on the contrary can be predicted by nuclear models, parametrized with average properties. Measured average cross sections can therefore finetune the parametrization of these models.

At even higher excitation energies, many more decay channels open up and cross

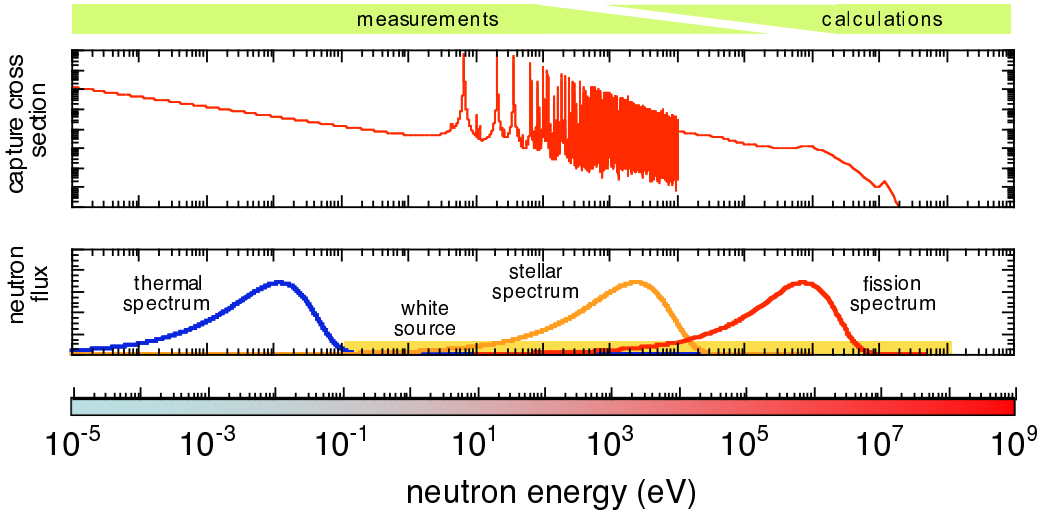

Figure 3: The neutron capture cross section of ^{238}U together with several different neutron source energy distributions in a wide energy range.

section measurements become very difficult or impossible. Reaction cross sections may therefore only be accessible by nuclear model calculations.

As an example, in figure 3 the neutron capture cross section of ^{238}U is shown on an energy scale spanning more than ten decades. The resonance structures, given by resonance paramters, are clearly visible in the low energy part while the smooth cross section at higher energies is parametrized in the libraries by interpolation tables. The sudden transition between these two regimes is therefore not physical but related to these different descriptions.

In order to appreciate the importance of the cross sections at different energies, typical energy distributions of neutron fluxes are also shown in the figure. The energy region around a few tens of meV is called the thermal region and is of importance in reactor physics where the by water moderated neutrons are in thermal equilibrium with the water and have Maxwell-Boltzmann distributed velocities peaked at an equivalent kinetic energy $k_B T$. For a temperature of nearly 300 K this corresponds to 25.3 meV or a velocity of 2200 m/s. The thermal cross section at 25.3 meV is an important quantity and can be measured accurately with only small amounts of material in reactor experiments.

A different energy distribution is found for neutrons in certain stars and responsible for the synthesis of the isotopes heavier than about $A = 60$ in the universe. The neutrons are present as a hot gas and also have a Maxwellian kinetic energy

distribution but now at temperatures with $k_B T$ ranging from 5 to 100 keV. Stellar nucleosynthesis will be briefly outlined later.

Several distribution functions describe in a satisfactory way the kinetic energy distribution of neutrons from the nuclear fission process. The neutrons from ^{235}U thermal neutron induced fission follow well a Maxwellian kinetic energy distribution, peaked at about 1 MeV. This distribution is also shown in figure 3.

In the resolved resonance region, which includes the thermal region, the reaction cross sections can be rigorously described in terms of resonance parameters, which are the properties of the excited states like energy, spin and parity. This is done by means of *R*-matrix theory, which is outlined in more detail in a next section. The advantage of the parametrization of resonant cross sections by the *R*-matrix formalism is that relatively few data are needed from which Doppler broadened cross sections at any temperature can be calculated.

The *R*-matrix description can be extended to the unresolved resonance region, where average resonance parameters can be adjusted to describe the cross sections. A related approach in this energy region and at higher energies is the use of optical model calculations. The interaction with the nucleus is then modelled by a complex potential well. By solving the Schrödinger equation one can calculate the cross sections. The difficulty lies in the parametrization of the potential.

Neutron induced reaction data are of great importance for nuclear reactor physics. In several other fields, including astrophysics and fundamental symmetries, neutron induced reactions play also an important role. Some items will be discussed in the following sections. In addition, important information on level densities, a key ingredient in many nuclear reaction codes, can be obtained directly from neutron resonance spectroscopy [8]. Many of the experimental data have been compiled [9–11] and once evaluated, made available through nuclear data libraries like BROND [12], ENDF-B [13], JEFF [14] and JENDL [15] and CENDL [16].

CHAPTER 1

Neutron data for science and technology

1.1 Parity nonconservation

Symmetry plays an important role in physics. It has been believed for a long time that all physical laws are invariant under the parity operation. The parity operation or space inversion **P** reverses the sign of all the spatial coordinates $\mathbf{r} \rightarrow -\mathbf{r}$. If the mirror system gives again a situation that obeys the same physical laws as the original system, then it is said to be invariant under parity. In fact, the gravitational, the electromagnetic and the strong interactions are all believed to be invariant under parity.

The principle of parity invariance was thought to be a general symmetry in nature, until Lee and Yang showed in 1956 that for the weak interaction no evidence for parity conservation existed and that there were reasons to believe that parity may not be conserved in the weak nuclear interaction. Indeed, Wu and her co-workers found in their famous experiment on the spatial asymmetry of the β-decay of polarized ^{60}Co nuclei that parity was not conserved in the weak interaction [17]. Many other experiments since then have confirmed the nonconservation of parity in leptonic weak interactions.

There are two more basic symmetry operations in addition to parity, namely charge conjugation **C** and time reversal **T**. The operation **C** consists of replacing each particle by its antiparticle and the operation **T** reverses the time and replaces in quantum mechanics the wave function by its complex conjugate. Nature is assumed to be invariant under the combined operations of **C**, **P** and **T**, which is known as the CPT-theorem. A test for CPT-invariance is the equality of the masses and lifetimes of a particle and its antiparticle. So far, no indications for the violation of CPT-invariance have been found [18]. The CPT-theorem implies that if one of the operators is not conserved, at least one of the other operators must also be not conserved. In the case of the weak process of nuclear β-decay, where parity is not conserved, also charge conjugation is not conserved. In the case of β^+-decay, the asymmetry of β-emission of polarized nuclei is opposite

to that of β^--decay as for example was shown for ^{58}Co and ^{52}Mn [19, 20]. The combined operation **CP** preserves here the symmetry.

Due to the weakness of the parity nonconserving interaction with respect to the strong nuclear parity conserving force, one expects under normal conditions only very small parity admixtures in nuclear levels. The weak hadronic PNC interaction acts as to add to the nuclear wave function a small fraction of a wave function with opposite parity

$$\Psi = \Psi^{(\pi)} + F\Psi^{(-\pi)} \tag{1.1}$$

where F is in the order of 10^{-7}, which is the relative strength of the weak parity nonconserving part of the nucleon-nucleon force as compared to the strong parity conserving interaction [21,22]. In several spectroscopy and reaction experiments it was found that parity nonconservation occurs up to about 10^{-3} [23,24]. It has been shown that parity nonconservation occurs extensively in compound nucleus formation by neutron capture due to specific enhancement factors, notably in epithermal neutron p-wave resonances. Since it is believed that the same amplification mechanisms may also hold for the violation of time reversal invariance, a thorough study of parity nonconservation in neutron p-wave resonances is, apart from its specific interest for the investigation of the weak interaction, essential for the possible direct observation of the violation of time reversal invariance.

The work of Abov *et al.* [25] demonstrated for the first time parity nonconservation in the neutron-nucleus system by detecting the asymmetry in the gamma-ray yield from an unpolarized ^{113}Cd sample using polarized thermal neutrons. These experiments and others pointed out that the PNC effects are associated to the compound nuclear levels. New investigations started looking for parity nonconservation in individual compound nucleus levels in the resonance region.

A significant enhancement of the PNC part may occur in highly excited compound nuclei due to the mixing of nuclear levels of the same (channel) spin and opposite parity. In heavy nuclei the combination of certain enhancements may amplify the PNC effects by a factor of 10^4 to 10^6. These effects are of two kinds. The relative small distance in energy between the two interfering states is referred to as dynamic enhancement, while a large difference in widths is called kinematic enhancement. Both factors are present in equation (1.3). Such enhanced PNC effects in p-wave resonances have been measured first in Dubna [26] and were followed by a large series of transmission measurements in Los Alamos by the TRIPLE collaboration with low-energy polarized neutrons using different nuclei for the unpolarized targets [27,28]. In these measurements PNC-effects as large as 10 % have been observed.

PNC-effects are particularly prominent in p-wave resonances and can be explained by the admixing of nearby s-wave resonances with the same channel spin. The

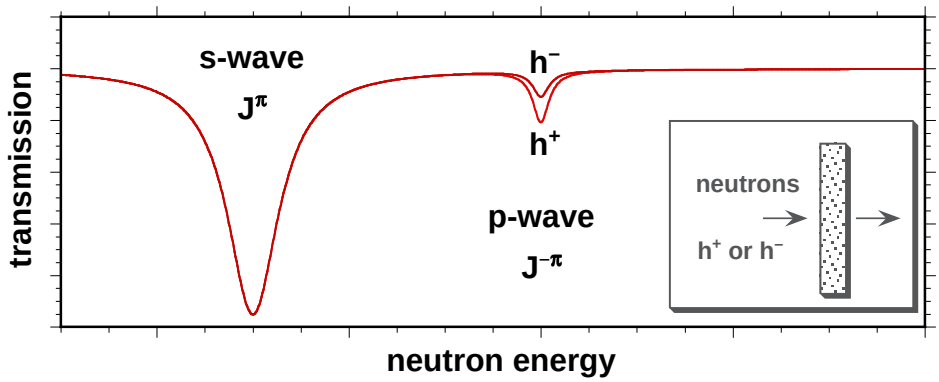

Figure 1.1: The transmission of a beam of longitudinal polarized neutrons through an unpolarized target depends at specific energies on the direction of polarization of the neutrons.

relative orbital momentum $\ell = 0$ and $\ell = 1$ for s- and p-wave resonances gives the opposite parity for the two nuclear states corresponding to the resonances.

This can be measured by polarizing a beam of neutrons longitudinally and observing the transmission through matter. The direction of polarization with respect to its momentum, the helicity $h^{\pm}$, can be reversed, which is equivalent to the parity operation. The neutron transmission at p-wave resonances differs according to the helicity. This may be illustrated as sketched in figure 1.1.

The parity nonconserving asymmetry P is defined as the relative difference of the measured cross sections $\sigma^{\pm}$ with the polarized neutron beam having positive or negative helicity

$$P = \frac{\sigma^+ - \sigma^-}{\sigma^+ + \sigma^-} \tag{1.2}$$

assuming a fully polarized beam. More precise expressions for polarized neutron reaction cross sections can be found in refs. [29,30]. For a spin zero target nucleus in a two-level approximation P can be described as

$$P = \frac{2V_{sp}}{E_s - E_p}\sqrt{\frac{\Gamma_n^s}{\Gamma_n^p}} \tag{1.3}$$

where V_{sp} is the PNC matrix element between s- and p-wave states and where Γ_n^s and Γ_n^p are the neutron widths for s- and p-wave resonances respectively. The small difference in energy of the two levels and the large difference in their neutron entrance channel widths, for p-waves typically a factor 10^3 smaller than for s-waves in this mass and energy region, have as a consequence that PNC effects are largest in low-energy neutron p-wave resonances of heavy and medium mass nuclei.

The matrix elements V_{sp} for the p-wave resonances, derived from the measured asymmetries and known resonance neutron widths and energies, are supposed to have a Gaussian distribution with zero mean and variance M^2. For the ensemble of p-wave resonances one can via a statistical analysis estimate the root mean squared value of the PNC matrix element $\sqrt{M^2}$ in nuclear matter, revealing the overall strength of the weak interaction in the nucleus.

PNC has been observed in neutron resonances of several target nuclei in the successful TRIPLE experiments at Los Alamos [27,28,31,32]. In general the deduced M-values are qualitatively consistent with the theoretical expectation. The case of ^{232}Th is an exception because the signs of the asymmetries of almost all resonances are positive. This deviation from the results for other nuclei suggests that the sign correlation observed in ^{232}Th is specific, and is not a general feature of the weak nucleon-nucleus interaction. A large number of possible theoretical explanations for this sign correlation have been worked out but so far none of them are really satisfactory [27].

An important aspect for the interpretation of the parity nonconservation is the knowledge of the resonance spins and the in particular the small p-wave resonances, which are generally unknown. In the case of a spin zero target nucleus, the s-waves have all spin $1/2$, while the p-wave resonances have either spin $1/2$ or $3/2$. Only the spin $1/2$ p-wave resonances can show parity nonconserving asymmetries. It is therefore important to know the resonance spins for a correct interpretation of the measured parity nonconserving asymmetries. Particular attention has been paid to spin assignments based on the population of low-lying levels by means of gamma-ray spectroscopy [31,33–35].

The resonance energies are rather well known. However, due to the small cross sections of low-energy p-wave resonances, little attention has been paid to them since they do not contribute significantly to multigroup cross sections. Their importance was mainly related to the understanding of the level density. A more precise knowledge of the p-wave neutron widths Γ_n may improve the extraction of the matrix elements V_{sp} from the measured asymmetries P and in this way improve the interpretation of these data.

Also other reactions are currently addressed in order to study parity nonconservation in lighter systems, notably using n(p,d)γ reactions [32,36].

1.2 Stellar nucleosynthesis

The origin of the chemical elements is an intriguing topic and the understanding of it helps to gain insight in the history of the universe. Hydrogen and helium, and small amounts of lithium, were formed in the time period between about 100 seconds and 30 minutes after the Big Bang [37]. This period of primordial nucleosynthesis was followed by galactic condensation and the formation of stars. All elements heavier than lithium have been formed in stars, and the elements heavier than iron have been formed by neutron capture processes. The isotopic abundances in the solar system reflect the average composition of the galaxy when as it was 4.5×10^9 ago. Spectral information of stellar environments and isotopic analyses of presolar dust grains provide important observations to validate stellar evolution models.

1.2.1 Stellar evolution

The classification of stars, clouds of gas massive enough to have nuclear reactions and to be bounded by gravitational attraction, is made by means of the Hertzsprung-Russell diagram, where the luminosity or brightness of a star is plotted against its surface temperature. The surface of a star emits nearly black body radiation with a corresponding spectral distribution, which has a dominant component on the blue spectral side for the hotter stars and on the red side for the cooler stars. The luminosity is related to the mass of the star.

Such a diagram reveals interesting patterns as shown in figure 1.2. First it can be distinguished that the positions of the stars are not randomly distributed and that more than 90% of the stars are on the so-called main sequence, a large band going from hot and bright for the heaviest stars to cooler and less luminous for the lighter stars. Note that the axis with temperature is decreasing, as historically it was represented by increasing wavelength. Above the main sequence are the red giants and supergiants. These stars are very luminous, but have a relatively low temperature on the surface. On the lower side of the main sequence are the white dwarfs, relatively small stars with a high surface temperature. The diagram is not a static situation. During the life of a star, its evolution follows a path trough the Hertzsprung-Russell diagram, starting somewhere on the main sequence where it stays for 90% of its life.

In a simple picture a star in its early life consists of a mixture of hydrogen and helium. The temperature increases due to the gravitational contraction and the Coulomb barrier for protons can be overcome to start fusion reactions building up ^{4}He. The radiation pressure counter-balances the gravitational force and the star is in equilibrium. Our Sun is at this stage like the majority of stars in the main sequence. If all hydrogen has been used the gravitational collapse starts again, increasing the temperature until the Coulomb barrier for the ^{4}He nuclei can be

overcome. The outer envelope of the star increases while the surface temperature decreases. In this phase the star has become a red giant.

At this stage carbon is formed through the 3 ^{4}He$\rightarrow^{12}$C reaction, possible as a consequence of the presence of a ^{12}C resonance at an excited state of 7.65 MeV. Subsequent (α,γ) reactions produce heavier nuclei with a decreasing amount because of the increasing Coulomb barrier for heavier isotopes. The less massive stars with masses up to a few Sun masses will end up as a hot carbon core which eventually cools down to become a white dwarf.

For more massive stars, when the ^{4}He fuel has been spent, the carbon core collapses from the gravitational force, increasing again the temperature of the star permitting fusion reactions of heavier nuclei. These chains of nucleosynthesis by charged particle reactions, in combination with photodissociation reactions, end at the $A = 56$ nuclei with a large abundance of ^{56}Fe. For heavier nuclei the charged particle fusion reactions are energetically not allowed anymore. The iron core may in its turn collapse until so high nuclear densities are reached that other infalling matter bounces off the core producing a supernova explosion.

Stars spend most of their lifes in the main sequence in the phase of burning hy-

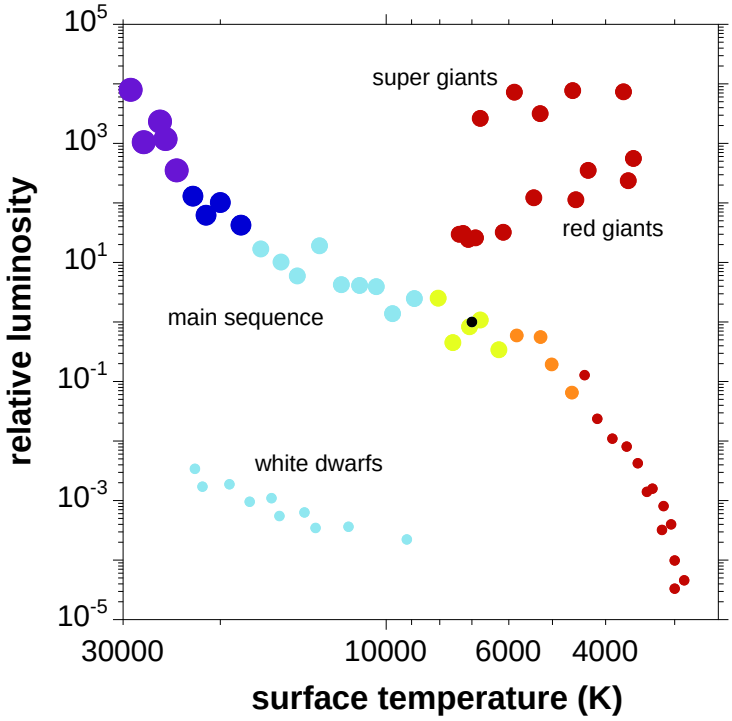

Figure 1.2: Schematic view of a Hertzsprung-Russell diagram.

drogen. At the end of their lifes when the hydrogen has been exhausted they leave the main sequence for the final phases of their evolution. The lifetime of a star depends very much on its mass. A small cool red star with a temperature of about 3000 K can have a lifetime as long as 1×10^{14} years, while a heavy supermassive star of 2×10^{4} K may live for only 1×10^{6} years. Our Sun with a surface temperature of 6000 K has a lifetime of about 8×10^{9} years.

1.2.2 The s-process

Stellar nucleosynthesis has first been extensively reviewed in the reference work [38] and more recently in ref. [39, 40]. The isotopes up to ^{56}Fe can be synthesized by fusion reactions during the different stages of evolution of a star. It is nowadays well established that neutron capture processes in red giant stars and supernovae are responsible for the formation of nearly all isotopes with higher masses [38, 41]. This was first recognized by the discovery of technetium in red giant stars [42]. The element Tc has no stable isotopes and the lifetimes are short compared to the stellar evolution times, proving that the element had been formed in the star.

The neutron capture mechanisms are known as the s-process and r-process, where "s" stands for slow and "r" for rapid referring to the time scale on which the neutron capture takes place. The neutrons needed for the neutron capture come mainly from the ^{22}Ne(α,n)^{25}Mg and ^{13}C(α,n)^{16}O reactions. The s- and the r-process are important for the stable and neutron rich isotopes. A thorough knowledge of the s-process, for which much more experimental data is available, constrains the possibilities of the r-process. A competing mechanism is the p-process, referring to photodisintegration reactions like (γ,n), (γ,p) and (γ,α). They influence the abundances from the proton rich side.

If the compound nucleus is unstable against beta decay, it may decay before it captures a second neutron. This is what happens in the s-process which is the principal process of synthesis in the red giant stars, where thousands of years may pass between two successive neutron captures on a nucleus. In this way many of the isotopes from ^{56}Fe to ^{209}Bi are formed. Heavier nuclei than bismuth are unstable and cannot be formed by neutron capture anymore. The s-process path follows closely the valley of stability in the chart of the nuclei and ends at ^{209}Bi.

In the r-process the neutron capture process is much faster and occurs on much shorter time scales. The time between consecutive neutron captures is in the order of seconds. In order to achieve the according extremely high neutron fluxes, the astrophysical site for the r-process is believed to be of explosive nature, like in a supernova. The competition between neutron capture and beta decay follows much longer sequences of successive neutron capture until the beta decay

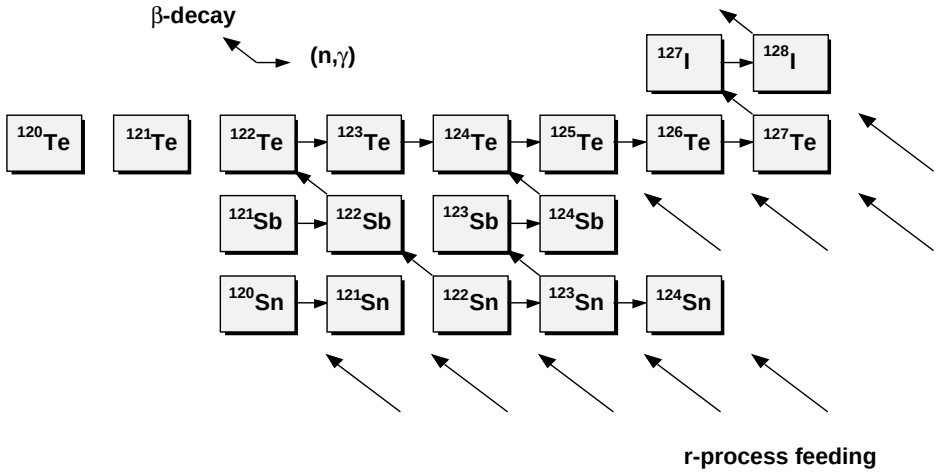

Figure 1.3: Simplified part of the s-process path in the Sn region with s-only and r-only isotopes as explained in the text, after [40].

half life is too short and the path follows the beta decay towards stability. Since the synthesis path of the r-process can go very far towards the neutron drip line before beta decay occurs, nuclei heavier than ^{209}Bi can be formed in this way. The actinides, which cannot be formed by the s-process, have been formed mainly by the r-process.

At a given point in the neutron capture chain the probability of beta decay and neutron capture may be comparable. This is a branching point in the synthesis path. Neutron capture cross sections are a key ingredient in the development of stellar models using the calculation of nuclear abundances in stellar environments. At the branching points uncertainties in the cross sections can propagate into large differences in the production of higher mass nuclei within a given model.

In a very schematic quantitative description of the s-process, starting from the seed nucleus ^{56}Fe and assuming constant temperature and neutron density, for a s-only nucleus the product of the average capture cross section $\langle\sigma_\gamma\rangle_{kT,A}$ and the abundance of the isotope $N_{s,A}$ is constant

$$\langle\sigma_\gamma\rangle_{kT,A}\, N_{s,A} = \text{constant}\,. \tag{1.4}$$

Indeed this is roughly the case, except for the nuclei with neutron magic numbers ($N = 28, 50, 82, 126$) around $A = 88$, 140, and 208, which have very low cross sections. These nuclei are bottlenecks in the s-process paths, and show up as abundance peaks. The s-only nuclei are shielded from the r-process by stable isobars of nuclei with lower Z and for which contributions from the proton rich side of the valley of stability are commonly neglected. In the same way r-only nuclei have no contribution from the s-process.

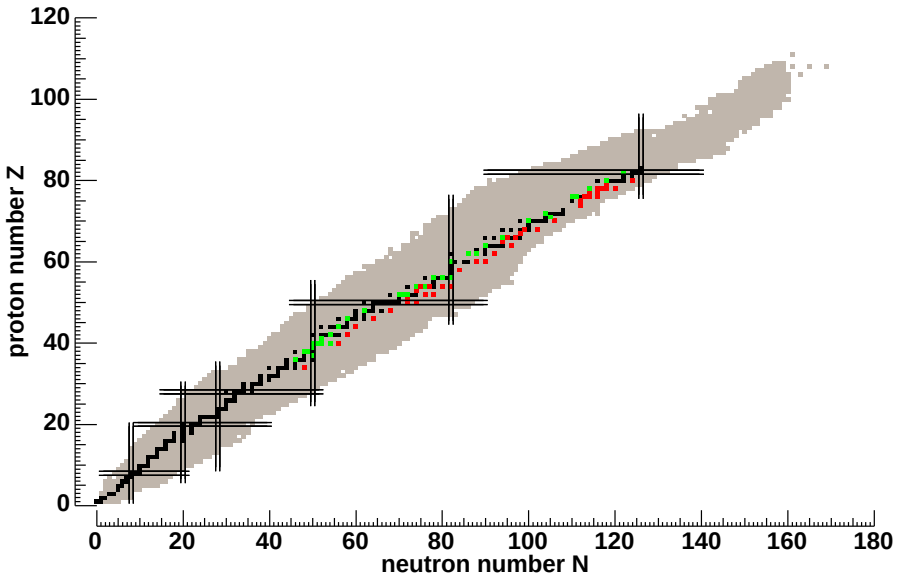

Figure 1.4: The chart of the nuclides showing the stable isotopes (data from [43]) along the s-process in black, and the s-only and r-only isotopes in green and red respectively (data from [44]).

In figure 1.3 a simplified part of the s-process is shown in the $Z = 50$ vicinity starting from ^{120}Sn. Some stable nuclides, like ^{124}Sn and ^{130}Te are not reached by the s-process path and are endpoints of r-process beta-decay cascades. These isotopes are called r-only isotopes. On the other hand, ^{122}Te, ^{123}Te and ^{124}Te are in the s-process path but are shielded from the r-process by the nuclei ^{122}Sb, ^{123}Sb and ^{124}Sb. These are s-only isotopes. The about 30 s- and about 40 r-only isotopes provide a means to distinguish between the two processes. They are given in figure 1.4 showing also the stable nuclides.

1.2.3 The Maxwellian-averaged neutron capture cross section

In the refinement of stellar models, the required input of neutron cross sections is needed in the form of cross sections averaged over the kinetic energy distribution of the neutrons.

Average neutron capture cross sections can be calculated from the energy dependent cross sections. In stellar environments, the relative velocities v between the neutrons and the target isotopes follow a Maxwell-Boltzmann distribution at a temperature T. The reaction rates are proportional to the Maxwellian-averaged neutron capture (MAC) cross section

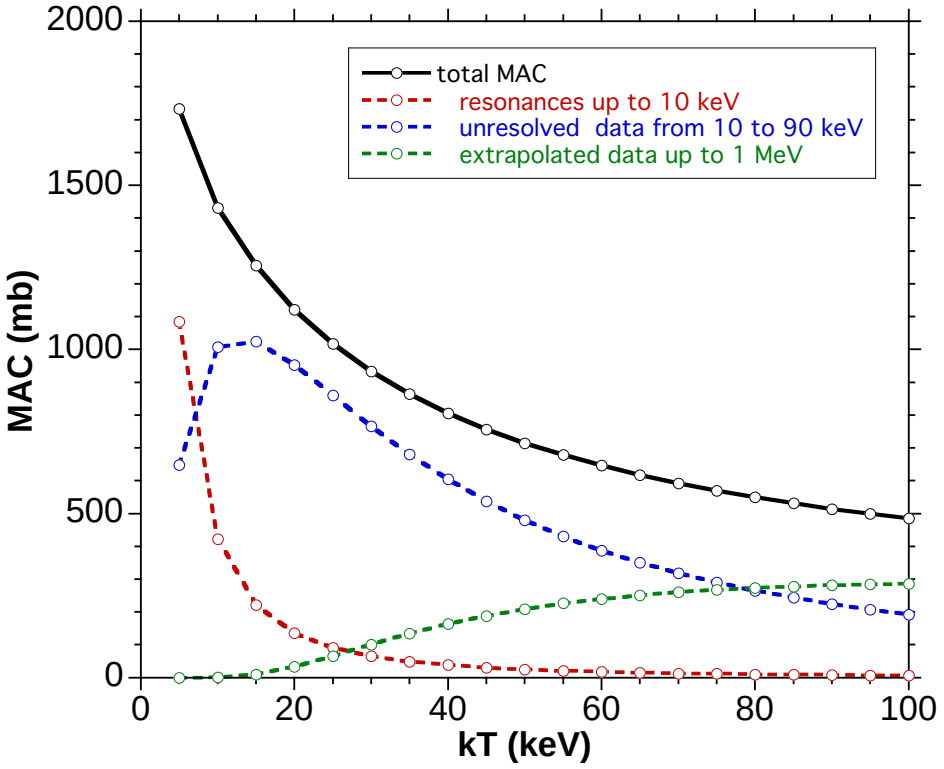

Figure 1.5: The Maxwellian averaged capture cross section for ^{99}Tc as a function of the stellar temperature. The contributions from both the resolved and unresolved resonance region are also given. Data are from [45].

$$\langle \sigma_\gamma \rangle_{kT} = \frac{\langle \sigma_\gamma v \rangle}{\langle v \rangle} = \frac{2}{\sqrt{\pi}(kT)^2} \int_0^\infty \sigma_\gamma(E) E \exp\left(-\frac{E}{kT}\right) dE \tag{1.5}$$

where $\sigma_\gamma(E)$ is the neutron capture cross section at energy E, which is the total kinetic energy of the center of mass system.

Relevant temperatures for current models range from $kT = 5$ keV to 100 keV. In figure 1.5 the MAC is shown for the radioactive nuclide ^{99}Tc as a function of the temperature [45]. The contribution of the resolved resonances in the cross section far below 5 keV is also given. Its importance is far from negligible at low stellar temperatures.

More sophisticated modelizations require also more detailed neutron cross sections to test stellar evolution models against observational data. Neutron cross section are known for many isotopes but the quality of the existing data is not

always sufficient, in particular for isotopes with small cross sections or for radioactive isotopes.

1.3 Nuclear data for nuclear energy

Within 50 years, the world's energy need is expected to double. In order to face this demand, a long term energy supply strategy is indispensable. At present about 80% of the energy production comes from fossil resources, coal, oil and gas [46, 47]. The known and exploitable reserves are thought to be exhausted in about 100 years for oil and gas, and in about 250 years for coal. This apparent abundance has for long inhibited a strong economic impulse for the search of alternative energy sources. Only recently global warming and the emission of green-house gasses like CO_2, related to the combustion of fossil energy sources, are of widely spread concern.

Other energy sources, like solar or wind energy, are in full technological development but can only satisfy a small fraction of the total energy need. Nuclear fusion is still in a research phase and its commercial exploitation is far beyond the near future.

Energy from nuclear fission is a well mastered technique today. In France, about 75% of the electricity production comes from nuclear energy. The nuclear energy production is about 40% in the European Union and 7% worldwide. In addition to non-proliferation concerns, a satisfactory solution of the nuclear waste problem is a necessary condition for the public acceptance of nuclear energy in the years to come.

Several research lines address this issue. Safe solutions for geological disposal are studied. Also considered, probably as a complementary solution, is the option of transmutation of nuclear waste. This consists of transforming the radioactive isotopes into stable or less radiotoxic isotopes via neutron capture and neutron fission reactions. Other options are the reduction of the long-term radiotoxic inventory of nuclear waste by using different fuel cycles in existing or new reactors, or specific devices dedicated to transmutation. A fuel cycle based on thorium, producing much less radiotoxic actinides is a promising alternative. Research activities exist on detailed studies of isotopic evolution in several deployment scenarios, but also on the basic nuclear data necessary for these applications [48–52].

In parallel, research is concentrated on the development of a future generation of nuclear power reactors, also known as Generation IV, to be operational by 2050. A number of six concepts have been retained for investigation, research and development, namely the Very High Temperature Reactor (VHTR), the Gas Cooled Fast Reactor (GFR), the Lead-Cooled Fast Reactor (LFR), the Sodium Cooled Fast Reactor (SFR), the Supercritical Water Cooled Reactor (SCWR), and the Molten Salt Cooled Reactor (MSR).

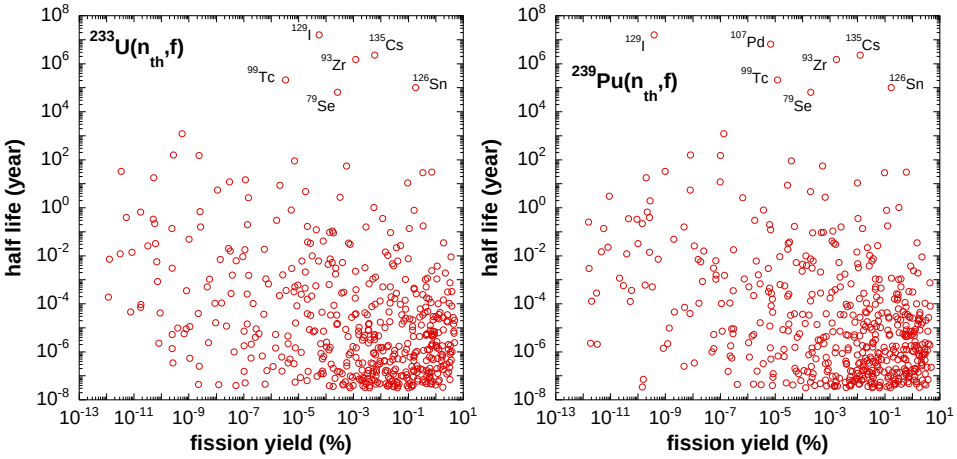

Figure 1.6: The spectrum of fission products produced with thermal neutrons on ^{233}U and ^{239}Pu. Data from [53].

1.3.1 Nuclear waste transmutation

Conventional nuclear power reactors are based on the fission process of ^{235}U and ^{239}Pu. While ^{235}U is fissile, the fertile uranium isotope ^{238}U becomes the fissile ^{239}Pu during the use of the fuel due to neutron capture followed by β-decay:

$$^{238}\mathrm{U} + \mathrm{n} \longrightarrow {}^{239}\mathrm{U} \xrightarrow{\beta^- \ (23\ min)} {}^{239}\mathrm{Np} \xrightarrow{\beta^- \ (2.4\ d)} {}^{239}\mathrm{Pu}\,. \tag{1.6}$$

The abundance of ^{235}U in natural uranium is about 0.7%. In order to be used in a thermal reactor an enrichment to about 3% is used in a typical reactor fuel, leaving a remaining 97% of ^{238}U.

A large range of fission products is generated with a wide variety of half lifes and yields. A plot of the half life versus the individual fission yield indicates clearly the long living fission products, as shown in figure 1.6.

On a relatively short time scale, the fission products will contribute most to the radiotoxicity. After longer periods, relatively few long living fission products are remaining. Transmutation can change the nuclear properties drastically as is illustrated by the fission product ^{99}Tc with a half life of $2 \cdot 10^5$ years. After capture of a neutron the formed nucleus ^{100}Tc decays with a half life of 15.8 s to the stable isotope ^{100}Ru. Taken also into account its ability to migrate in storage glasses, makes ^{99}Tc a particularly suited candidate for transmutation. Its neutron induced reaction cross sections have been investigated recently [45, 54].

Table 1.1: Inventory of the yearly production in France of the most important long living fission products and minor actinides, considered as nuclear waste . Numbers from [55].

isotope	production (kg/year)	half life year
^{79}Se	5	$1.1 \cdot 10^6$
^{93}Zr	800	$1.5 \cdot 10^6$
^{99}Tc	900	$2.1 \cdot 10^5$
^{107}Pd	200	$6.5 \cdot 10^6$
^{126}Sn	20	$1.0 \cdot 10^5$
^{129}I	200	$1.6 \cdot 10^7$
^{135}Cs	400	$2.3 \cdot 10^6$
^{237}Np	500	$2.1 \cdot 10^6$
^{241}Am	250	432
^{243}Am	100	7370
^{244}Cm	25	18.1
^{245}Cm	1.5	8500

The large amount of ^{238}U in the fuel is the basis of the production of the highly radiotoxic actinides by successive neutron captures and beta decays, leading to the formation of isotopes of Pu, Am and Cm. In table 1.1 the composition of the nuclear waste produced per year in France is given.

The transmutation process can take place in a high neutron flux environment provided by thermal reactors, fast reactors or Accelerator Driven Systems (ADS) consisting of a high energy proton accelerator, a spallation target and a subcritical core [56, 57]. ADS systems have an increased passive safety as compared to conventional critical reactors. They have been proposed in a large variety of kinds. In many design studies a liquid core of lead and bismuth is considered, acting as a spallation neutron source. The use of ADS systems has been proposed in configurations for waste transmutation but also for energy production in combination with thorium-based fuel.

A large worldwide research programme on nuclear data in the second half of the 20th century has permitted the construction of vast databases of continuously growing quality. For a precise assessment of the transmutation rates in given neutron fluxes with given energy spectra as well as for criticality and safety calculations due to the introduction in the reactor cores of quantities of isotopes to be transmuted, accurate values of the relevant cross sections are still needed. Since today's nuclear power reactors are all based on the uranium cycle, important lacks exist in nuclear data for these new applications.

1.3.2 The thorium cycle

In currently operating nuclear fission reactors the spent fuel elements account for the largest part of nuclear waste in terms of radiation activity. Apart from uranium, the waste consists of fission products and isotopes of plutonium and minor actinides like neptunium, americium and curium. After a cooling period of the spent fuel to diminish the activity due to the shorter lived fission products, the remaining material is, after a possible extraction of the uranium and plutonium, considered as waste. The high activity and long lifetimes of several isotopes necessitates a long term storage under safe conditions on a time scale surpassing generations. Transmutation of these isotopes by means of neutron capture of fission, could considerably reduce the radiotoxicity inventory.

An other approach is to reduce the amount of nuclear waste, notably the higher actinides, by using a fuel cycle based on ^{232}Th, see for example refs. [56, 57] for detailed concepts. The isotope ^{232}Th itself is not fissile but after neutron capture followed by β-decay, the fissile isotope ^{233}U is formed. The build-up of the higher actinides, especially americium and curium, is strongly suppressed due to the lower atomic and mass number of thorium.

The alternative fuel cycle is based on the use of thorium in nuclear reactors. In this cycle ^{233}U is the fissile isotope which is formed from ^{232}Th by neutron capture followed by β-decay

$$^{232}\mathrm{Th} + \mathrm{n} \longrightarrow {}^{233}\mathrm{Th} \xrightarrow{\beta^- \ (22\ min)} {}^{233}\mathrm{Pa} \xrightarrow{\beta^- \ (27\ d)} {}^{233}\mathrm{U}\,. \tag{1.7}$$

An interesting advantage from the point of view of production of radioactive waste in using the ^{232}Th/^{233}U-based fuel cycle as compared to the classic uranium cycle is related to its low production in of higher mass actinides. The lower atomic number of thorium with $Z = 90$, instead of $Z = 92$ for uranium, reduces significantly the build-up of heavy transuranium isotopes, in particular plutonium and curium. This is also clearly demonstrated by detailed simulations on the isotopic composition of a thorium-based ADS system [58]. In figure 1.7 a schematic view of the isotope formation in the thorium cycle is shown.

In addition other arguments play a role. The natural abundance of thorium is three times larger than that of uranium so extends potentially the existing fuel resources. Also the number of neutrons produced after absorption of a neutron in a reactor environment is larger for ^{233}U than for ^{235}U or ^{239}Pu for thermal neutrons, opening the possibility, although technically still quite complicated, for a "thermal breeder".

Several experimental projects using thorium have already been worked out in the

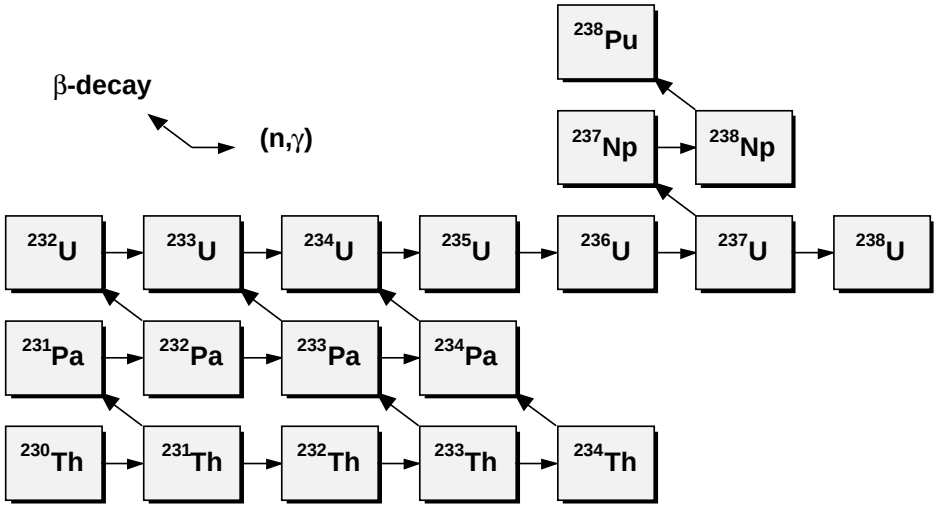

Figure 1.7: The actinide production chain for the thorium fuel cycle.

past on critical assemblies (Molten Salt Reactor, CANDU-Th, High-Temperature Gas Reactor). Due to encountered technical problems but also overshadowed by the rapid industrialized production of uranium-based reactors, a long history of research and development has been focussed on the uranium based cycle, which is nowadays the standard for all operating power plants, and is at present missing for thorium.

The growing concern of the public opinion on nuclear waste and inherently safely operating nuclear energy systems has led to a variety of research activities. The use of thorium in the nuclear fuel cycle for either critical or subcritical systems is nowadays a topic of interest.

Recently, many developments and studies have been devoted to subcritical reactors driven by an accelerator. Such an ADS has clear advantages on the criticality and safety aspects of nuclear energy production as compared to critical assemblies and opens new perspectives for nuclear waste management [56, 57]. This type of reactors can be used to incinerate radioactive waste (primarily long-lived minor actinides), to burn the massive stocks of plutonium, or to produce energy in an efficient and safe way. An innovative concept using an ADS with ^{232}Th/^{233}U is the Energy Amplifier [59].

The present state of the description of the thorium-cycle related cross sections is not yet at the level of that of the uranium cycle. The conceptualization and realization of nuclear power stations based on the use of thorium, either in a critical or subcritical system, require a good knowledge of the reaction cross sections of the thorium cycle isotopes. As indicated in "The NEA high priority nuclear data request list" [60], the capture cross section of ^{232}Th with uncertainties smaller

than 5% are needed in the region between 1 eV and 500 keV. A precision of even 1-2% for ^{232}Th and somewhat less stringent up to 5-10% for ^{231}Pa, ^{234}U and ^{236}U is requested in a dedicated study on nuclear data needs for the thorium fuel cycle [61,62].

These new applications have triggered a renewed interest in neutron-nucleus reactions in particular for isotopes and energy regions of isotopes essential for the development and efficiently optimized design of the above mentioned concepts. Indeed many of the relevant isotopes have received less attention in the past and at present the existing measured data are still insufficient, incomplete or sometimes even lacking.

As an example we mention the recent large effort of several groups to measure the neutron induced cross sections on the important isotope ^{232}Th [63–69].

1.4 Neutron data libraries

Historically, the interaction of neutrons with nuclei has been for long of primary interest for conventional nuclear reactor physics. The industrial constraints concerning safety and criticality but also modelization and development, have lead to the development of standardized formats of nuclear data for storage and retrieval of evaluated nuclear data. An evaluated data set for a particular isotope needs to be complete for the application it is used for. This means that the evaluator has to combine experimentally measured cross section data with predictions of nuclear model calculations in order to obtain a single complete data set. The evaluated data set is adopted in the library after extensive benchmarking and reviewing. In figure 1.8 the isotopes included in the 4 most important libraries are displayed. An evaluated library, like JEFF (Europe) [14], JENDL (Japan) [15], ENDF/B (United States) [13], BROND (Russia) [12] or CENDL (China) [16], contains several sublibraries, each one corresponding to a particular type of data. As a result of including other specific purpose libraries, not only incident neutron data are present, but also incident charged particle data, photo-nuclear data and several other types of data.

The evaluated data sets in the libraries concern items that are called materials, each identified by a material number. The most natural materials are nuclides,

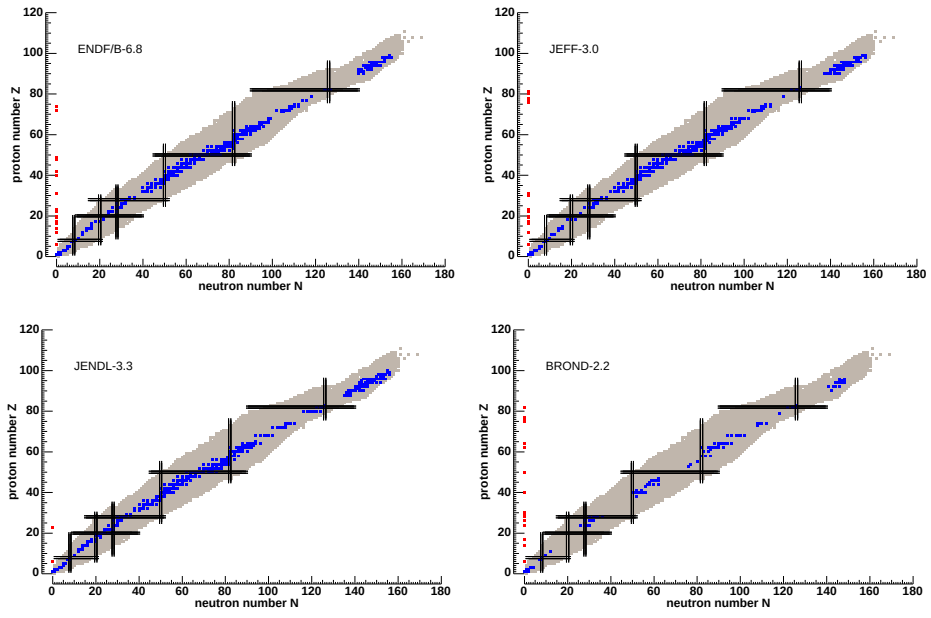

Figure 1.8: Isotopes included in the important neutron data libraries JEFF, JENDL, ENDF/B and BROND.

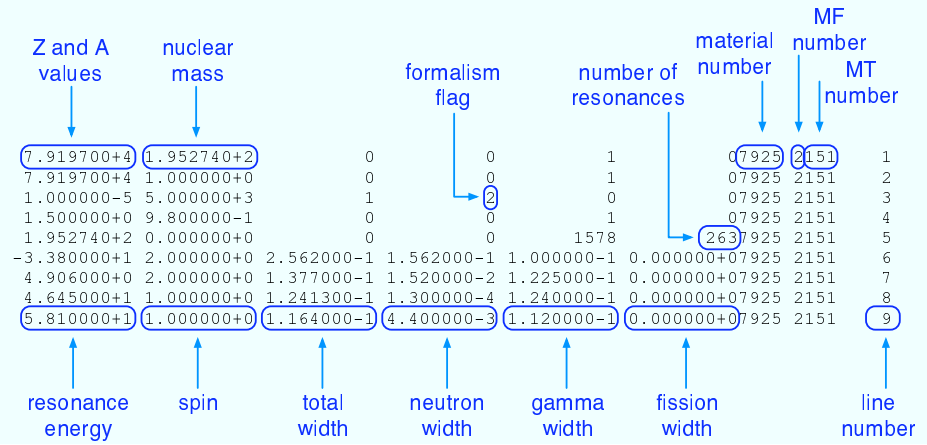

Figure 1.9: Part of the neutron data on ^{197}Au from JEFF-3.0.

possibly in a metastable state, for which the nuclear reaction parameters correspond to physical properties. But also natural elements or even compounds are allowed. With time and more accurate nuclear data the tendency in modern evaluated libraries is to remove as much as possible compounds and natural elements and include only isotopes and metastable states. Each material in an incident-neutron sublibrary has several "files", flagged by a file number known as MF, containing for example general information (MF=1 or file 1), resonance parameter data (file 2), point-wise cross section in the form of interpolation tables (file 3), angular and energy distributions, multiplicities, radioactivity and fission-product yield data, covariance information and many other data resulting in about 40 files. Not all files are mandatorily present in an evaluated data file. The files contain indicators, the so-called MT numbers, giving further specification. For example for point-wise cross sections (MF=3), MT=1 represents the total cross section, MT=2 the elastic scattering cross section, MT=18 the total fission cross section and MT=102 the capture cross section.

The data are represented according to strict formatting rules, the ENDF format, documented in [70]. This format, originally only for the ENDF library, has been adopted for all other libraries as well. As an example in figure 1.9 a small part of the data corresponding to resonance parameters (file 2) for the isotope ^{197}Au is given. Evaluated libraries are the basic input to be processed by codes as NJOY [71] or PREPRO [72] to extract the data and put them for example in the form of Doppler broadened or group averaged cross section in a format useable by transport codes. New data needs or newly available experimental data may lead to new evaluations. An updated library can be released only when the full library has passed extensive testing, giving coherent results in benchmarks on a variety of applications like reactor criticality calculations.

1.5 Statistical model observations

In the approximation of the statistical model, as already mentioned in the introduction, the properties of the nuclear levels in the compound nucleus excited by incident neutrons have typical characterics resulting from the random nature of matrix elements governing the nuclear transitions [1–5].

A correct understanding of the neutron resonance observables and their distributions is of importance for for example the derivation of level densities. All level density models are adjusted in order to match the level density at the neutron binding energy. Level spacings at high excitation energies are nearly exclusively derived from neutron resonance spectroscopy. The statistical distributions of the neutron widths and the level spacings can be used to obtain reliable estimates for the level density accounting for the effects of missing levels [54, 73].

1.5.1 Partial width fluctuations

Within the statistical model the matrix elements corresponding to transitions between states are supposed to have random amplitudes γ having a Gaussian distribution with zero mean. The observed channel widths are related to the amplitudes by $\Gamma_c = 2P_\ell\gamma_c^2$. By removing the energy dependence, one can define the reduced channel widths for a given value of ℓ by

$$\Gamma_c^\ell = \frac{P_0}{P_\ell}\sqrt{\frac{1\text{ eV}}{E}}\Gamma_c \tag{1.8}$$

Expressions for P_ℓ are given in table 2.2 on page 49. As a consequence, the reduced channel widths Γ_c^ℓ are related to a chi-squared distribution with one degree of freedom $\nu = 1$

$$P(\chi^2,\nu) = \frac{1}{2^{\nu/2}\Gamma(\nu/2)}(\chi^2)^{(\nu/2-1)}\exp(\chi^2/2) \tag{1.9}$$

where $\Gamma(\nu/2)$ is the gamma function and $\nu = 1$. For the neutron channel, indeed the reduced neutron widths have been found to follow such a distribution. The distribution for the normalized reduced neutrons widths $x = \Gamma_n^0/ < \Gamma_n^0 >$ for $\ell = 0$ resonances is also called the Porter-Thomas distribution

$$P_{\text{PT}}(x) = \frac{1}{\sqrt{2\pi x}}\exp\left(-\frac{x}{2}\right) \tag{1.10}$$

Instead of matching this distribution with observed data, it is more convenient to use a kind of reverse cummulative distribution and compare the number of resonances with a value of x larger than a threshold value x_t

$$N(x_t) = N_0\int_{x_t}^{\infty} P_{\text{PT}}(x)dx = N_0(1-\text{erf}\sqrt{x_t/2})\,. \tag{1.11}$$

The value N_0 gives the real number of resonances in the energy region considered. At low thresholds resonances are generally missing and the data deviates from the expectation. At higher threshold values, the observed data should be in agreement with the integrated distribution. This is illustrated in figure 1.10.

For other reaction channels, the situation is different since the observables are more often the sum of several channels. In fission for example, an effective degree of freedom between 2 and 4 has be found. For capture, the radiation width can be the sum of tens of thousands of partial radiation widths, each corresponding to a particular gamma-ray transition.

1.5.2 Level spacings

Another consequence of the random nature of the compound nucleus is the distribution of the spacing D between two consecutive levels of the same spin and ℓ value. This next-neighbour level spacing, sometimes confusingly and wrongly called neirest-neighbour level spacing, can be described by the Wigner distribution

$$P_W(x) = \frac{\pi}{2} x \exp\left(-\frac{\pi}{4}x^2\right) \tag{1.12}$$

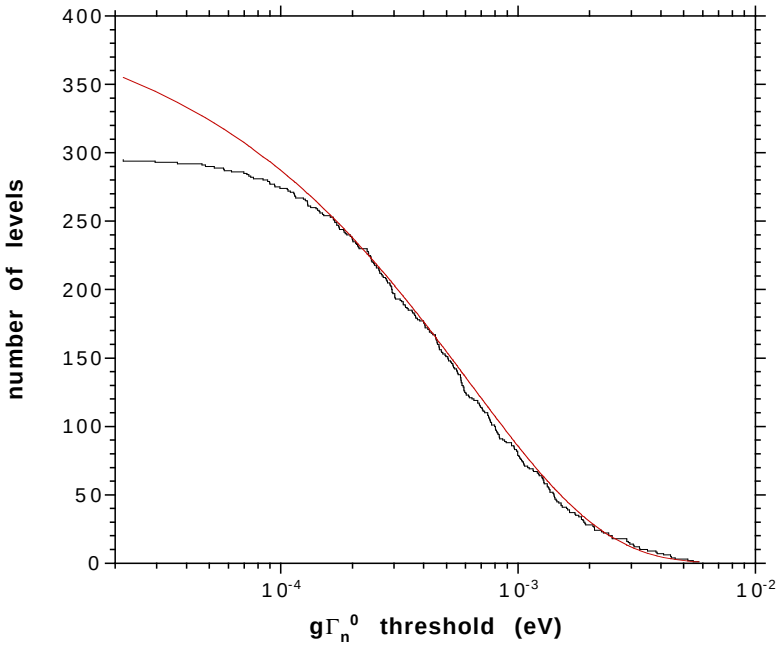

Figure 1.10: An example of the integrated number of levels above a threshold value of the neutron width together with the prediction of equation (1.11).

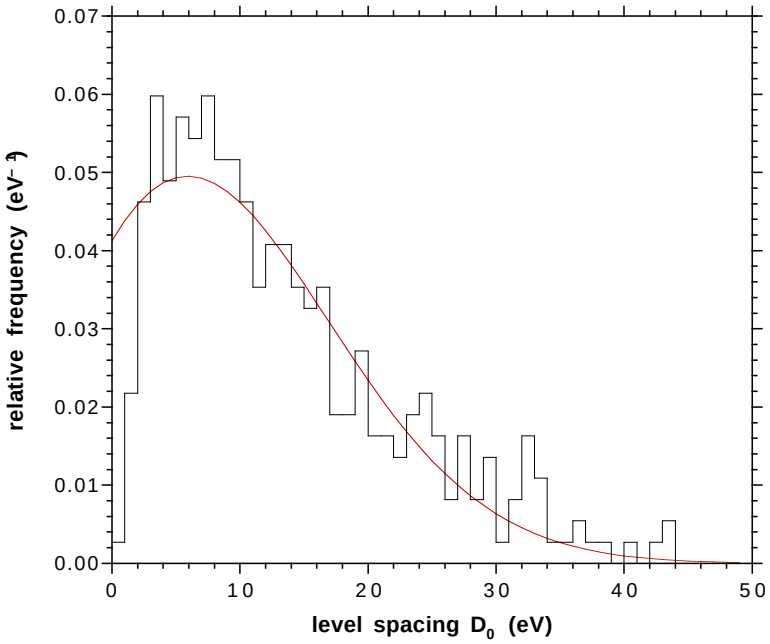

Figure 1.11: The level spacing distribution of a sequence of spin $J = 4$ and $J = 5$ resonances from [54]. The smooth curve is not a fit but the theoretical expectation.

with $x = D/ < D >$. An interesting feature is that the spacing distribution goes to zero for small x. This is known as the level repulsion effect, reflecting the fact that small spacings are less likely. For level spacing distributions consisting of a mixed spin sequence, the resulting distribution is a much more complicated expression [1] and does not go to zero anymore for small spacings. Not observed small spacings are then corresponding to non resolved resonances. In figure 1.11 an example for resonances with a mixture of spin $J = 4$ and $J = 5$ levels.

1.6 Neutron cross section measurements

1.6.1 Experimental facilities

For measurements of neutron induced cross sections several neutron sources can be used. Reactor neutrons are widely used in experiments to determine Maxwellian averaged cross sections in the thermal region. Low mass samples in the range of micrograms are sufficient. At higher energies, typically in the MeV range, nearly monochromatic neutrons or a broader spectrum can be obtained by means of an accelerator producing neutrons via light particle reactions like ^{7}Li(p,n)^{7}Be or ^{9}Be(α,n)^{12}C. This results in cross section measurements at specific neutron energies or cross sections averaged over a tailored neutron spectrum.

For high-resolution neutron spectroscopy, a neutron source covering a large energy range is most convenient. Accelerator-based pulsed white neutron sources are suitable for this purpose. A moderator of a material rich in hydrogen can be applied in order to increase the amount of low-energy neutrons. Such machines can provide a neutron energy spectrum ranging from several meV up to several hundreds of MeV. It is necessary that the source is pulsed because the selection of the neutron energy is determined by the time-of-flight method. Such pulsed neutron sources are realized using electron- and proton-based accelerators.

The electron-based sources produce neutrons via Bremsstrahlung. The cross section for this process is approximately proportional to Z^2, thus favouring photoproduction for heavy mass nuclei. The photons induce photonuclear reactions (γ,n) and, if the target is fissionable, photofission reactions (γ,f). Around about 10-20 MeV the cross sections for photodisintegration reactions increase considerably due to the giant dipole resonance and are approximately proportional to NZ/A, thus again favouring targets of heavy mass nuclei. Examples of white pulsed neutron sources are GELINA of the EC-JRC-IRMM at Geel in Belgium, using 140 MeV electrons incident on a uranium target [74–76], ORELA at Oak Ridge National Laboratory, using 180 MeV electrons on a tantalum target, the RPI facility at Troy (USA) or KURRI at Kyoto.

The proton-based machines produce neutrons as secondary particles in reactions in the MeV region up to about 100 MeV. At higher incident proton energies neutrons are produced by the spallation process with a very high yield of neutrons per proton striking a target of heavy nuclei. Examples are the LANSCE facility at Los Alamos National Laboratory, with 800 MeV protons and the spallation source at KEK in Tokyo. A more recent construction is the n_TOF facility at CERN with 20 GeV protons on a lead target [69,77–85].

1.6.2 The neutron time-of-flight method

In order to perform neutron time-of-flight measurements, it is important that the neutron source is pulsed. In a relatively short time, typically a few nanoseconds, the neutrons with a broad energy spectrum are created at the reference start time t_0. At a distance L ranging from a few meters to several hundreds of meters for high resolution experiments, a target is placed in the neutron beam. For reaction cross sections, the reaction product, like fission fragments, alpha particles, capture gamma rays or scattered neutrons are detected. These cross sections are usually normalized by a reference measurement on a known standard target in the same experimental conditions. Total cross sections are addressed by measuring the neutron beam attenuation. The neutron flux is measured alternatingly with a sample in and out of the neutron beam. No reference sample is needed for this type of experiment since the measurements give the absolute total cross section.

The time of detection t_n of the reaction product serves as a stop signal to determine the time of flight $t = t_n - t_0$ of the neutron having induced the reaction. The kinetic energy E_n of neutrons with a speed $v = L/t$ can be expressed relativistically as

$$E_n = E_{tot} - mc^2 = c^2p^2 + m^2c^4 - mc^2 = mc^2(\gamma - 1) \tag{1.13}$$

with $\gamma = (1 - v^2/c^2)^{-1/2}$ and where c is the speed of light. The first term of the series expansion gives the classical expression for the neutron kinetic energy

$$E_n = \frac{1}{2}mv^2 = \alpha^2\frac{L^2}{t^2}\,. \tag{1.14}$$

Taking the definition of the speed of light $c = 299792458$ m/s and taking $m = 939.6$ MeV$/c^2$ for the neutron mass, we get $\alpha \approx 72.3$ when L is expressed in meters and t in microseconds.

1.6.3 Experimental considerations

The reaction yields that are obtained in this way are, after background corrections, not directly related to the cross section formulae. The resonance profiles are broadened by two effects: Doppler broadening and resolution broadening.

The fraction of incident neutrons on a sample with thickness n atoms per barn, undergoing a reaction, is given by the reaction yield $Y_r(E) = R(E)/\Phi(E)$ where $R(E)$ is the reaction rate and $\Phi(E)$ the incident particle rate. In a first approximation the reaction yield is related to the cross sections by

$$Y_r(E) = \left(1 - e^{-n\sigma_T(E)}\right)\frac{\sigma_r(E)}{\sigma_T(E)} \tag{1.15}$$

where $\sigma_r(E)$ is the reaction cross section and $\sigma_T(E)$ the total cross section. In experiments at non-zero temperature the cross sections need to be convolved with Doppler broadening.

Doppler broadening is the effect of the thermal motion of the target nuclei in their atomic structure. Due to the movement of the target nucleus, a neutron approaching the nucleus with constant speed in the laboratory system, will have a spread in its velocity in the center of mass system. In a good approximation, for metallic samples this movement can be described by the free gas model [86], resulting in a Gaussian broadening of the resonances with a standard deviation

$$\sigma_D = \sqrt{\frac{2k_BT}{M/m}E} \tag{1.16}$$

with M/m the ratio of the masses of the target nucleus and the incident particle. For crystalline lattices a more complicated description is sometimes needed [87, 88]. Doppler broadening is always present in the interaction of neutrons with liquids or solids and cross sections are usually given at a specific temperature.

In addition to the Doppler broadening of the cross sections, the reaction yield is broadened by the experimental resolution. Resolution broadening is an experimental effect and reflects the distributions in the neutron flight time or flight length, originating from the finite primary beam pulse duration, the moderation distance, and all other experimental conditions. These effects are different for each experimental facility and have to be carefully modelled and included in the resonance analyses [89].

For thick samples, typically for capture reactions, also the effect of multiple scattering has to be taken into account. This concerns the fact that there is a non-negligible probability that the incident particle scatters from a nucleus in the sample and reacts afterwards with another nucleus in the sample. This effect depends not only on the cross sections but also on the sample geometry.

The two broadening effects are important for resolved resonances. For unresolved resonances, where the cross sections appear smooth, broadening has not much effect. On the contrary, since a resonance structure is still present, one cannot extract in a straightforward way the average cross section from the average yield, as can be seen from equation (1.15) by taking averages. The factor $\left(1 - e^{-n\sigma_T(E)}\right)$ gives rise to what is known as the self-shielding effect. Corrections based on Monte Carlo simulations have to applied for both the multiple scattering and the self-shielding effect.

CHAPTER 2

The R-matrix formalism

2.1 Introduction

The cross sections in neutron-nucleus reactions show large fluctuations of several orders of magnitude even for small changes of the neutron kinetic energy. The large peaks correspond to excitations of eigenstates in the compound nucleus. In order to describe the cross sections in a satisfactory way, the *R*-matrix formalism is the most accurate way.

The *R*-matrix theory has been first introduced by Wigner and Eisenbud [90]. A most extensive and detailed overview has been given by Lane and Thomas [91] and by Lynn [1]. Recently Fröhner [92] summarized the *R*-matrix formalism together with other useful considerations on nuclear data evaluation. Other related references of interest can be found elsewhere [93–101]. In the following only a brief outline of the formalism is given in order to understand the principle without giving the full details.

If the wave functions of the nuclear system before and after the reaction were known, one could calculate the cross section with the usual concepts of reaction theory. Where the incoming waves are known, the reaction modifies the outgoing wave functions in a generally unknown way.

The idea behind the *R*-matrix formalism is to use the wave function of the nuclear system of two particles when they are so close that they form a compound nucleus. Although the wave function of the compound nucleus is extremely complicated, one can expand it in its eigenstates. Matching then the incoming and outgoing waves to the internal wave function provides a way to describe the cross section of the reaction in terms of the properties of the eigenstates of the compound nucleus. These properties are basically the energy, spin, parity, and a set of partial widths related to the widths of the decay modes of the compound nucleus.

This method of describing a reaction cross section using only the properties of nuclear excitation levels, is at the same time also the most important limitation. No information of the forces inside the nucleus are needed or can be extracted.

The nucleus is treated as a black box of which the properties of the eigenstates have to be measured in order to describe the cross sections.

The binary nuclear reactions proceeding from one system of two particles to another system of two particles can be described with the general R-matrix theory. For neutron induced reactions, but also in other cases, such a reaction goes often through the formation of a compound nucleus X^*.

$$A + a \rightarrow X^* \rightarrow B + b \tag{2.1}$$

The R-matrix formalism does not only apply to compound nucleus reactions. Both direct and indirect reactions can be described with it. The inclusion of the Coulomb interaction allows to use it also for charged particle reactions. But the theory is applicable only in a general way for binary reactions which is appropriate for neutron induced reactions up to energies of several tens of MeV.

In a very general way, the cross section of a two-body nuclear reaction could be calculated if the nuclear wave functions were known. The wave functions could be calculated by solving the Schrödinger equation for the nuclear system. This requires that the nuclear potential is known. When the two particles are far away, the interaction can be considered absent for neutral particles or to be the Coulomb interaction for charged particles. In these cases it is indeed possible to calculate the wave functions.

When the two particles are so close to each other that a nuclear reaction takes place, the potential of the interaction is extremely complicated. For certain energy ranges and reactions this potential can still be approximated or calculated [102] and the wave functions and cross sections can be calculated. In other cases however, and especially in the resolved resonance region, the complexity of the reacting system does not allow this.

The first step is to consider that the reaction process can be split up geometrically into two regions for each channel where a channel is the precise constellation of particles and their spins. If the separation is smaller than the channel radius a_c, all nucleons involved in the reaction are close to each other and form a compound nucleus. Although the wave function of the compound nucleus is extremely complicated, it can be expanded as a linear combination of its eigenstates without solving explicitly the Schrödinger equation of the system. In the external region, at distances larger than a_c, the potential is zero for neutral particles or is the Coulomb interaction for charged particles and the Schrödinger equation of the system can be solved. The properties of the eigenstates of the compound nucleus are taken together in the R-matrix. Equating the values and derivatives of the wave functions at the boundary of the internal and external region assures a smooth wave function and the cross sections can be calculated. The exact internal wave function is not needed, only the values and derivatives at the nuclear surface.

2.2 Channel representation

It is customary to use the concept of channels in the description of nuclear reactions, which will be limited to two particle reactions in the following. The entrance channel c consists of a particular initial constellation of particles and all the quantum numbers necessary to describe the corresponding partial wave function. The type of the two particles α_1 and α_2, with their spins I_{α_1} and I_{α_2}, and their states of internal excitation are denoted by α. Four quantum numbers are needed to include the spins of the particles in a channel. The most appropriate combination is the orbital momentum ℓ, the channel spin j, which is the combined spin of the two particles

$$\mathbf{j} = \mathbf{I}_{\alpha_1} + \mathbf{I}_{\alpha_2}\,, \tag{2.2}$$

the total angular momentum J

$$\mathbf{J} = \mathbf{j} + \ell \tag{2.3}$$

and its projection on the z-axis m_J. So the entrance channel c can be designated by the set

$$c = \{\alpha, \ell, j, J, m_J\} \tag{2.4}$$

Similarly, the exit channel is given by

$$c' = \{\alpha', \ell', j', J', m'_J\} \tag{2.5}$$

The reaction $\alpha \rightarrow \alpha'$ may go through the formation of a compound nucleus, like often the case with neutron induced reactions. The reaction can then be written as $\alpha \rightarrow A^* \rightarrow \alpha'$. The spin and parity are of course conserved in all stages of the reaction and the compound nucleus has its defined spin J and parity π. The conservation of spin and parity puts restrictions on the entrance channels that are open to form the compound nucleus or the exit channels open for the decay of the compound nucleus. For neutrons and protons the intrinsic spin is $1/2$ and the intrinsic parity is positive. Conservation of angular momentum gives the vector addition:

$$\mathbf{J} = \mathbf{I}_{\alpha_1} + \mathbf{I}_{\alpha_2} + \ell = \mathbf{I}_{\alpha'_1} + \mathbf{I}_{\alpha'_2} + \ell' \tag{2.6}$$

and conservation of parity gives, using $+1$ for positive and -1 for negative parity:

$$\pi = \pi_{I_{\alpha_1}} \times \pi_{I_{\alpha_2}} \times (-1)^{\ell} = \pi_{I_{\alpha'_1}} \times \pi_{I_{\alpha'_2}} \times (-1)^{\ell'} \tag{2.7}$$

The boundary $r = a_c$ is the limit between the internal region, where there is an unknown potential and the wave functions can not be found by solving the Schrödinger equation, and the external region, where the potential is known (zero or Coulomb) and the wave functions can be calculated. Although there is no sharp limit, in practice the channel radius a_c can be taken just slightly larger than the nuclear volume with $A = A_{\alpha_1} + A_{\alpha_2}$ nucleons

$$a_c = R_0 A^{1/3} \tag{2.8}$$

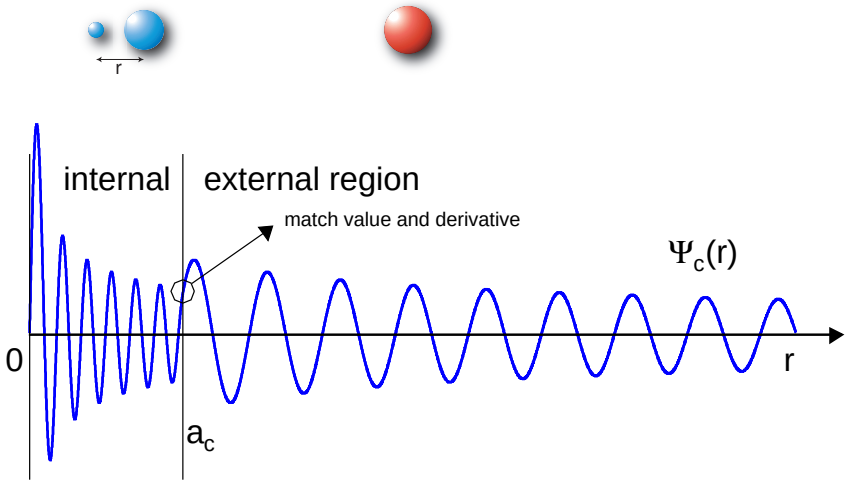

Figure 2.1: Schematic view of the wave function of a channel as a function of the separation distance r. The wave function in the internal region $r < a_c$ is an expansion of the eigenstates of the compound nucleus. The wave function in the external region $r > a_c$ is related to the Bessel functions. At $r = a_c$ the value and derivative of the wave function match.

The standard numerical value for a_c in the nuclear libraries is

$$a_c = 0.8 + 1.23A^{1/3} \text{ fm} \tag{2.9}$$

The channel is defined in the center of mass and the reduced mass of the particles is

$$m_c = m_\alpha = \frac{m_{\alpha_1} m_{\alpha_2}}{m_{\alpha_1} + m_{\alpha_2}} \tag{2.10}$$

and the wave number k, related to the de Broglie wavelength $\lambda\!\!\!^{-}$, is

$$k_c = k_\alpha = \frac{1}{\lambda\!\!\!^{-}_c} = \sqrt{\frac{2m_\alpha E_\alpha}{\hbar^2}} \tag{2.11}$$

and the relative velocity is

$$v_c = v_\alpha = \hbar k_c / m_c \tag{2.12}$$

The dimensionless distance ρ_c is used to indicate the distance r_c in measures of de Broglie wavelengths.

$$\rho_c = \rho_\alpha = k_c r_c \tag{2.13}$$

2.3 The wave function in the external region

The system of the two particles interacting through a central potential $V(r)$ can be described by the Schrödinger equation of the motion of the reduced mass particle. Also, using spherical coordinates, the solution $\psi(r,\theta,\phi)$ can, in case of a central potential, be separated in a radial and an angular part

$$\psi(r,\theta,\phi) = R(r)\Theta(\theta)\Phi(\phi) \tag{2.14}$$

The radial part $R(r)$ although still depends on the non-negative integer solutions $\ell(\ell+1)$ of $\Theta(\theta)$. The integers appearing in the solution of $\Phi(\phi)$ are $m_\ell = 0, \pm 1, \pm 2 \ldots \pm \ell$. The solutions of the angular part $\Theta(\theta)\Phi(\phi)$ do not depend on the central potential and are the spherical harmonics $Y^\ell_{m_\ell}(\theta,\phi)$. Only the solution $R(r)$ of the radial part depends on the potential $V(r)$. The radial Schrödinger equation

$$\left[\frac{d^2}{dr^2} - \frac{\ell(\ell+1)}{r^2} - \frac{2m_c}{\hbar^2}(V(r)-E)\right] R(r) = 0 \tag{2.15}$$

can be solved for the case of the Coulomb potential $V(r) = -Z_{\alpha_1}Z_{\alpha_2}e^2/(4\pi\epsilon_0 r)$. The general solution is a linear combination of regular and irregular Coulomb wave functions. In the special case that $V(r) = 0$, like for neutrons, equation (2.15), after a rearrangement in dimensionless form, is called the spherical Bessel equation. The solution consists of a linear combination of spherical Bessel functions of the first type $j_\ell(\rho)$, and of the second type $n_\ell(\rho)$ (or Neumann functions). Two linearly independent complex combinations of j_ℓ and n_ℓ are known as spherical Bessel functions of the third type (or Hankel functions) $h^+_\ell(\rho)$ and $h^-_\ell(\rho)$. These are functions of the dimensionless parameter $\rho = kr$. Although $n_\ell(\rho) \to -\infty$ for $r \to 0$, this irregular solution should be included because we only need this solution in the external region $r > a_c$. The appropriate solution for a channel c is a linear combination of waves corresponding to incoming $I_c(r)$ and outgoing $O_c(r)$ waves for a free particle, $R(r) = R_\ell(r) = y_\ell I_\ell(r) + x_\ell O_\ell(r)$, with

$$I_c(r) = I_\ell(r) = -i\rho h^-_\ell(\rho) = -i\rho\left[j_\ell(\rho) - i n_\ell(\rho)\right] \tag{2.16}$$

$$O_c(r) = O_\ell(r) = -i\rho h^+_\ell(\rho) = i\rho\left[j_\ell(\rho) + i n_\ell(\rho)\right] \tag{2.17}$$

At large separation distances $r \to \infty$ the asymptotic forms of $I(r)$ and $O(r)$ correspond indeed to plain waves travelling in positive direction (outgoing waves) or negative direction (incoming waves). The functions $j_\ell(\rho)$ and $n_\ell(\rho)$ together with $O_\ell(\rho)$ are given in table 2.1

2.4 The collision matrix U

The total wave function Ψ in the external region can be expressed as the superposition of all incoming and outgoing partial waves $\mathcal{I}_c$ and $\mathcal{O}_c$, with amplitudes

Table 2.1: The spherical Bessel functions and the incoming and outgoing waves from equation (2.17). Derived quantities are given in table 2.2.

ℓ	j_ℓ	n_ℓ	$O_\ell = I_\ell^*$
0	$\frac{\sin\rho}{\rho}$	- $\frac{\cos\rho}{\rho}$	$e^{i\rho}$
1	$\frac{\sin\rho}{\rho^2} - \frac{\cos\rho}{\rho}$	$-\frac{\cos\rho}{\rho^2} - \frac{\sin\rho}{\rho}$	$e^{i\rho}\left(\frac{1}{\rho} - i\right)$
ℓ	$(-1)^\ell\rho^\ell\left(\frac{1}{\rho}\frac{d}{d\rho}\right)^\ell\frac{\sin\rho}{\rho}$	$-(-1)^\ell\rho^\ell\left(\frac{1}{\rho}\frac{d}{d\rho}\right)^\ell\frac{\cos\rho}{\rho}$	

y_c and x_c, and summed over all possible channels c.

$$\Psi = \sum_c y_c \mathcal{I}_c + \sum_{c'} x_{c'} \mathcal{O}'_c \tag{2.18}$$

The complete wave functions in the channel, $\mathcal{I}_c$ and $\mathcal{O}_c$, contain the radial parts I_c and O_c, but also the angular part of relative motion $Y^\ell_{m_\ell}$, as well as the internal wave functions of the particles and the channel spin, combined in φ_c.

$$\mathcal{I}_c = I_c r^{-1}\varphi_c i^\ell Y^\ell_{m_\ell}(\theta,\phi)/\sqrt{v_c}\mathcal{O}_c = O_c r^{-1}\varphi_c i^\ell Y^\ell_{m_\ell}(\theta,\phi)/\sqrt{v_c} \tag{2.19}$$

The factor $1/\sqrt{v_c}$ normalizes the waves to unit flux. The physical process of the reaction will result in a modification of the outgoing waves. In the reaction the coefficients x_c of the outgoing waves, depending on the details of the reaction which are observable in the cross section, have to be determined with respect to the coefficients of the incoming waves y_c. The collision matrix $U_{cc'}$ is now defined as the relation between the coefficients of the incoming and outgoing waves:

$$x_{c'} \equiv -\sum_c U_{c'c} y_c \tag{2.20}$$

All the physics of the reaction is contained in the elements of the collision matrix. The collision matrix has two important properties. From the conservation of probability flux in the reaction is follows that the collision matrix it is unitary, which means that its complex conjugate equals its reciprocal, $\mathbf{U}^* = \mathbf{U}^{-1}$ or

$$\sum_c U^*_{cc'} U_{cc''} = \delta_{c'c''} \tag{2.21}$$

The second property follows from the conservation of time reversal conservation and implies that the collision matrix is symmetric, $U_{cc'} = U_{c'c}$.

Finally we can express the total wave function of equation (2.18) in terms of the collision matrix:

$$\Psi = \sum_c y_c \left(\mathcal{I}_c - \sum_{c'} U_{cc'}\mathcal{O}_{c'}\right) \tag{2.22}$$

which is a linear combination of the wave functions for each channel c, consisting of an ingoing wave and the modified outgoing waves summed over all channels c'.

2.5 The relation between the cross sections and the collision matrix U

The relation between reaction cross section and wave functions, describing a probability, is based on the conservation of probability density. The probability density of an incident plain wave, which is the flux of particles j is given by the quantum mechanical expression

$$j = \frac{\hbar}{2mi}\left(\psi^* \nabla\psi - \psi\nabla\psi^*\right) \tag{2.23}$$

The connection with the cross section is best illustrated by considering a flux of incident particles j_{inc}, represented by a plain wave ψ_{inc} which can be expanded in a series of partial radial waves, scattering elastically at a point $r = 0$ because of an unknown physical process. The scattered wave, originating at $r = 0$ is a radial wave ψ_{sc} and far from the scattering center at a distance r in a solid angle element $d\Omega$ the current of scattered particles across the surface $r^2 d\Omega$ is j_{sc}. The total wave $\psi = \psi_{\text{inc}} + \psi_{\text{sc}}$ is a solution of the Schrödinger equation for this system. The cross section of this reaction, which is a differential cross section, is defined as

$$d\sigma = \frac{j_{\text{sc}}}{j_{\text{inc}}} r^2 d\Omega \tag{2.24}$$

Integrating over $d\Omega$ gives the total scattering cross section. If elastic scattering were the only process to occur, the total current of ingoing particles equals that of the outgoing particles. Any reaction, defined as any other process than elastic scattering, will make that there is a difference in the absolute values of the ingoing and outgoing current.

In the more general description of channels the total wave function is equation (2.22). Elastic scattering means here that the entrance and exit channel are the same. A change of channel in the outgoing wave is considered as a reaction. With a similar approach, using the full description of the channel wave functions, the angular differential cross section for the reaction $\alpha \rightarrow \alpha'$ has been worked out by Blatt and Biedenharn [103]. For zero Coulomb interaction the expression is

$$\frac{d\sigma}{d\Omega} = \frac{1}{2j+1}\lambda\!\!\!^{-2} \sum_{\ell=0}^{\infty} B_\ell(c,c') P_\ell(\cos\theta) \tag{2.25}$$

The coefficients $B_\ell(c,c')$ are rather complicated factors and contain the collision matrix elements $U_{cc'}$ and relations containing Clebsch-Gordan coefficients for the spin bookkeeping, eliminating most of the terms in the infinite sum over ℓ.

The cross section for an interaction from channel c to channel c' is then

$$\sigma_{cc'} = \pi \lambda\!\!\!^{-2}_c |\delta_{c'c} - U_{c'c}|^2 \tag{2.26}$$

If the interaction occurs without a change in the channel c then the process is called elastic scattering. The cross section is, putting $c' = c$

$$\sigma_{cc} = \pi \lambda\!\!\!^{-2}_c |1 - U_{cc}|^2 \tag{2.27}$$

and the cross section for a channel reaction, i.e. any interaction which is not elastic scattering, is obtained by summing (2.26) over all c' except c

$$\sigma_{cr} = \pi \lambda\!\!\!^{-2}_c (1 - |U_{cc}|^2) \tag{2.28}$$

and the total cross section is obtained by summing all channels c'

$$\sigma_{c,T} = \sigma_c = 2\pi \lambda\!\!\!^{-2}_c (1 - \mathrm{Re}\, U_{cc}) \tag{2.29}$$

In practise, channel to channel cross sections are not useful. One would like to have the cross sections of $\alpha \to \alpha'$ for the component of total angular momentum J. The total reaction cross section is obtained by integrating equation over the full solid angle to obtain to total cross section for the component of total angular momentum J

$$\sigma_{\alpha\alpha'}(J) = \pi \lambda\!\!\!^{-2}_\alpha g(J) \sum_{j,j',\ell,\ell'} |\delta_{jj'\ell\ell'} - U_{j\ell,j'\ell'}|^2 \tag{2.30}$$

and the total cross section by summing over all α'

$$\sigma_{\alpha,T}(J) = 2\pi \lambda\!\!\!^{-2}_\alpha g(J) \sum_{j,\ell} (1 - \mathrm{Re}\, U_{j\ell,j\ell}) \tag{2.31}$$

2.6 The wave function in the internal region

2.6.1 Surface functions

The complete wave function Ψ can be described as the product of the function of relative motion and the channel-spin function, giving the internal states of the particles α_1 and α_2 and their combined spin. From the function of relative motion the radial part $R(r)$ is separated and the remaining part is combined with the channel-spin function to give the channel surface function φ_c

$$\Psi = \sum_c \varphi_c R_c(a_c)\,. \tag{2.32}$$

The surface functions φ_c have the property of orthonormality over the surface S_c given by $r = a_c$. This will be exploited to expand certain quantities in terms of surface functions. It follows immediately that

$$R_c(a_c) = \int \varphi_c^* \Psi dS_c\,. \tag{2.33}$$

The integration over a surface, instead of integrating over a volume, is particularly useful in deriving the R-matrix relation using Green's theorem, expressing a volume integral in a surface integral.

At the channel surface $r = a_c$ the radial wave function for the internal and external region should match. The value V_c and derivative D_c are defined with a normalization constant as

$$\begin{aligned} V_c &= \sqrt{\frac{\hbar^2}{2m_c a_c}} u_c(a_c) \\ &= \sqrt{\frac{\hbar^2}{2m_c a_c}} \int \varphi_c^* \Psi dS_c \end{aligned} \tag{2.34}$$

and

$$\begin{aligned} D_c &= \sqrt{\frac{\hbar^2}{2m_c a_c}} a_c \left(\frac{du_c}{dr}\right)_{r=a_c} \\ &= \sqrt{\frac{\hbar^2}{2m_c a_c}} \int \varphi_c^* \nabla_{\mathrm{n}} (r\Psi) dS_c \\ &= V_c + \sqrt{\frac{\hbar^2}{2m_c a_c}} a_c \int \varphi_c^* dS_c \end{aligned} \tag{2.35}$$

2.6.2 Internal wave functions

In the internal region the wave function cannot be calculated readily by solving the Schrödinger equation since the nuclear potential is in general very complicated. But the wave function can be expressed as an expansion in eigenfunctions X_λ and eigenvalues E_λ

$$\Psi = \sum_\lambda A_\lambda X_\lambda \tag{2.36}$$

and the coefficients A_λ can be expressed as

$$A_\lambda = \int X_\lambda^* \Psi d\tau \tag{2.37}$$

where the integration goes over the volume $d\tau$ of the internal region given by $r < a_c$.

The values and derivatives on the surface $r = a_c$ are defined, analog to equation (2.34) and (2.35), as

$$\gamma_{\lambda c} = \sqrt{\frac{\hbar^2}{2m_c a_c}} \int \varphi_c^* X_\lambda dS_c \tag{2.38}$$

and

$$\delta_{\lambda c} = \gamma_{\lambda c} + \sqrt{\frac{\hbar^2}{2m_c a_c}} a_c \int \varphi_c^* \nabla_{\mathrm{n}}(X_\lambda) dS_c \,. \tag{2.39}$$

The boundary conditions to be satisfied on the channel surface are taken identical for all λ

$$B_c = \delta_{\lambda c} / \gamma_{\lambda c} \,. \tag{2.40}$$

Applying Green's theorem to equation (2.37) gives

$$\begin{aligned} A_\lambda &= \int X_\lambda^* \Psi d\tau \\ &= (E_\lambda - E)^{-1} \frac{\hbar^2}{2m_c} \int (X_\lambda^* \nabla_{\mathrm{n}}(\Psi) - \Psi \nabla_{\mathrm{n}}(X_\lambda^*))\, dS_c \\ &= (E_\lambda - E)^{-1} \sum_c (D_c - B_c V_c) \gamma_{\lambda c} \end{aligned} \tag{2.41}$$

using equations (2.34), (2.35), (2.38), (2.39) and (2.50). The expression (2.36) for the wavefunction can now be written as

$$\Psi = \sum_c \left[\sum_\lambda \frac{X_\lambda \gamma_{\lambda c}}{E_\lambda - E} \right] (D_c - B_c V_c) \,. \tag{2.42}$$

By multiplying each side of equation (2.42) by $\varphi_{c'}$, integrating over the surface $r = a_c$ and using equation (2.38) one obtains

$$V_{c'} = \sum_c R_{cc'} (D_c - B_c V_c) \tag{2.43}$$

with

$$R_{cc'} = \sum_\lambda \frac{\gamma_{\lambda c} \gamma_{\lambda c'}}{E_\lambda - E} \,. \tag{2.44}$$

The quantity $R_{cc'}$ is the R-matrix and contains the properties E_λ and $\gamma_{\lambda c}$ of the eigenstates λ. The boundary constant B_c can be chosen freely.

2.7 The relation between the R-matrix and the collision matrix U

The values and derivatives of the internal wave function are given by the R-matrix relation equation (2.43). The external wave function is given by equation (2.22) and is known except for the boundary conditions. The boundary condition is that both the internal and external wave functions have the same value and radial derivative at $r = a_c$ in order to have a smooth transition. By matching these conditions and after considerable rearrangements, the collision matrix $U_{cc'}$ can be given explicitly as a function of the R-matrix in matrix notation by

$$\mathbf{U} = \mathbf{\Omega} \mathbf{P}^{1/2} [\mathbf{1} - \mathbf{R}(\mathbf{L} - \mathbf{B})]^{-1} [\mathbf{1} - \mathbf{R}(\mathbf{L}^* - \mathbf{B})] \mathbf{P}^{-1/2} \mathbf{\Omega} \,. \tag{2.45}$$

The introduced complex matrix **L** is given by

$$L_c = S_c + iP_c = \left(\frac{\rho}{O_c}\frac{dO_c}{d\rho}\right)_{r=a_c} \tag{2.46}$$

where real matrices S_c is called the shift factor and P_c the penetrability factor. The matrix Ω_c is

$$\Omega_c = \left(\frac{I_c}{O_c}\right)_{r=a_c} \tag{2.47}$$

which can be reduced for neutral particles, using equation (2.17), to

$$\Omega_c = \exp(-i\phi_c) \tag{2.48}$$

from which ϕ_c follows

$$\phi_c = \arg O_c(a_c) = \arctan\left(\frac{\operatorname{Im} O_c}{\operatorname{Re} O_c}\right) = \arctan\left(-\frac{j_\ell(\rho)}{n_\ell(\rho)}\right) \tag{2.49}$$

All matrices in equation (2.45) are diagonal matrices except **U** and **R**. A table of P_ℓ, S_ℓ and ϕ_ℓ is given below. They are directly related to the solution of the Schrödinger equation in the external region, which are the spherical Bessel and Neumann functions $j_\ell(\rho)$ and $n_\ell(\rho)$ for neutral particles, and can be derived from the quantities listed in table 2.1.

If the boundary conditions B_c, defined by equation (2.50), are real, then the $\delta_{\lambda c}$ and the $\gamma_{\lambda c}$ are real and hence **R** is real. In addition **R** is symmetrical. A common choice is to take

$$B_c = S_c \tag{2.50}$$

which eliminates the shift factor for s-waves, but introduces an energy dependence. The choice $B_c = -\ell$ has also been proposed [92].

Table 2.2: The penetrability P_ℓ, the level shift S_ℓ and the hard-sphere phase shift ϕ_ℓ for reaction channels without Coulomb interaction, as a function of $\rho = ka_c$. These parameters are derived from the quantities in table 2.1.

ℓ	P_ℓ	S_ℓ	ϕ_ℓ
0	ρ	0	ρ
1	$\rho^3/(1+\rho^2)$	$-1/(1+\rho^2)$	$\rho - \arctan\rho$
ℓ	$\frac{\rho^2 P_{\ell-1}}{(\ell-S_{\ell-1})^2+P_{\ell-1}^2}$	$\frac{\rho^2(\ell-S_{\ell-1})}{(\ell-S_{\ell-1})^2+P_{\ell-1}^2} - \ell$	$\phi_{\ell-1} - \arctan\frac{P_{\ell-1}}{\ell-S_{\ell-1}}$

So equation (2.45) defines the collision matrix in terms of the parameters of the R-matrix, $\gamma_{\lambda c}$ and E_λ, representing the physical process of the reaction, and the

quantities P_c, S_c, ϕ_c, describing the known incoming and outgoing waves I_c and O_c, outside a sphere with radius a_c. The values B_c determine the boundary conditions at the matching point of the internal and external region, and are free to be chosen. The unknowns of the R-matrix, $\gamma_{\lambda c}$ and E_λ, need to be determined in order to know the U-matrix and subsequently the cross sections.

2.8 Approximations of the R-matrix

Several approximations of the R-matrix have been developed in the past in order to overcome the complications of inverting the matrix

$$[\mathbf{1} - \mathbf{R}(\mathbf{L} - \mathbf{B})]^{-1}$$

appearing in equation (2.45). Except in the case where only 1 or 2 channels are involved, the inversion is in general impossible without additional assumptions. The problem can be put in terms of the inversion of a level matrix $\mathbf{A}$ of which the elements refer to the properties of the levels λ of the system. The problem of inverting a matrix concerning all channels is now put in a problem of inverting a matrix concerning levels. The level matrix $A_{\lambda\mu}$ is introduced by putting the following form

$$\left([\mathbf{1} - \mathbf{R}(\mathbf{L} - \mathbf{B})]^{-1}\right)_{cc'} = \delta_{cc'} + \sum_{\lambda\mu} \gamma_{\lambda c}\gamma_{\mu c'}(L_{c'} - B_{c'})A_{\lambda\mu} \tag{2.51}$$

from which the elements of the inverse of $\mathbf{A}$ are

$$\begin{aligned}\left(\mathbf{A}^{-1}\right)_{\lambda\mu} &= (E_\lambda - E)\delta_{\lambda\mu} - \sum_c \gamma_{\lambda c}\gamma_{\mu c}(L_c - B_c) \\ &= (E_\lambda - E)\delta_{\lambda\mu} - \Delta_{\lambda\mu} - \frac{1}{2}i\Gamma_{\lambda\mu}\end{aligned} \tag{2.52}$$

with the quantities $\Delta_{\lambda\mu}$ and $\Gamma_{\lambda\mu}$ defined by

$$\Delta_{\lambda\mu} = \sum_c (S_c - B_c)\gamma_{\lambda c}\gamma_{\mu c} \tag{2.53}$$

and

$$\Gamma_{\lambda\mu} = 2\sum_c P_c\gamma_{\lambda c}\gamma_{\mu c} \tag{2.54}$$

Now the collision matrix from equation (2.45) can be expressed in terms of $\mathbf{A}$

$$U_{cc'} = \Omega_c\Omega_{c'}\left(\delta_{cc'} + 2i\sqrt{P_cP_{c'}}\sum_{\lambda\mu} A_{\lambda\mu}\gamma_{\lambda c}\gamma_{\mu c'}\right) \tag{2.55}$$

Additional approximations have been formulated in order to simplify this expression. The most illustrative is the Breit and Wigner Single Level (SLBW) approximation where only one level is considered. It can be extended to several,

independent levels, which is the Breit and Wigner Multi Level (MLBW) approximation. The formalism of Reich and Moore [104] neglects only the off-diagonal contributions of the photon channels, which is an accurate approximation for medium and heavy nuclei. It takes into account the interference between levels and reduces to the BWSL approximation in the limit of a single level. These three formalisms will be described in some more detail. Other formalisms exists of which we mention here the formalisms of Kapur and Peierls [105], Wigner and Eisenbud [90], Adler and Adler [96], Hwang [106] and more recently Luk'yanov and Yaneva [100].

2.8.1 The Breit-Wigner Single Level approximation

The expression equation (2.52) can be simplified if only a single level is present. In that case the matrix contains only a single element. Therefore

$$\left(\mathbf{A}^{-1}\right)_{\lambda\mu} = A^{-1} = E_\lambda - E + \Delta_\lambda - i\Gamma_\lambda/2 \tag{2.56}$$

with

$$\Delta_\lambda = \Delta_{\lambda\lambda} = -\sum_c (S_c - B_c)\gamma_{\lambda c}^2 \tag{2.57}$$

and

$$\Gamma_\lambda = \Gamma_{\lambda\lambda} = \sum_c \Gamma_{\lambda c} = \sum_c 2P_c\gamma_{\lambda c}^2 \tag{2.58}$$

Substituting these expressions in equation (2.55) gives the collision matrix

$$U_{cc'} = e^{-i(\phi_c+\phi_{c'})}\left(\delta_{cc'} + \frac{i\sqrt{\Gamma_{\lambda c}\Gamma_{\mu c'}}}{E_\lambda + \Delta_\lambda - E - i\Gamma_\lambda/2}\right) \tag{2.59}$$

From the collision matrix the cross sections can be calculated. For the total cross section this results in

$$\sigma_c = \pi\lambda\!\!\!^{-2}_c g_c\left(4\sin^2\phi_c + \frac{\Gamma_\lambda\Gamma_{\lambda c}\cos 2\phi_c + 2(E - E_\lambda - \Delta_\lambda)\Gamma_{\lambda c}\sin 2\phi_c}{(E - E_\lambda - \Delta_\lambda)^2 + \Gamma_\lambda^2/4}\right) \tag{2.60}$$

The first part of the total cross section is the potential scattering or hard sphere scattering cross section $\sigma_p = 4\pi\lambda\!\!\!^{-2}_c g_c \sin^2\phi_c$. It is associated with the elastic scattering of the incoming neutron from the potential of the nucleus without forming a compound state. The term with the factor $\sin 2\phi_c$ is the interference of the potential scattering and the resonant elastic scattering through formation of a compound nucleus. Finally the term with $\cos 2\phi_c$ describes the resonance cross sections of the channels.

In a more practical case we can see what the cross sections becomes for a neutron entrance channel $c = n$. We assume that the only open channels are elastic scattering and neutron capture, $\Gamma_\lambda = \Gamma = \Gamma_n + \Gamma_\gamma$.

A series expansion of the trigoniometric factors gives for $\ell = 0$ in good approximation $\sin\phi_c = \rho = ka_c$ and $\sin\phi_c = 0$ for $\ell > 0$. The cosine term can be approximated by $\cos\phi_c = 1$ for all ℓ.

In the same way, the reaction cross section is

$$\sigma_{cc'} = 4\pi\lambda\!\!\!^{-2}_c g_c \frac{\Gamma_{\lambda c}\Gamma_{\lambda c'}}{(E - E_\lambda - \Delta_\lambda)^2 + \Gamma_\lambda^2/4} \tag{2.61}$$

and the shift Δ_λ results from the boundary condition.

2.8.2 The Breit-Wigner multi level approximation

Several resonances can be taken into account as a sum of Breit and Wigner single level cross sections. This is the most simple treatment of cross sections of many resonances. It neglects any possible interference between channels and levels (resonances).

The Breit and Wigner multi level (BWML) approach uses a sum over the levels in the collision matrix. In the inverse of the level matrix $\mathbf{A}$ all off-diagonal elements $A_\lambda^{-1}\mu$ are neglected, which means neglecting all interference terms between channels, but not between levels.

$$\left(\mathbf{A}^{-1}\right)_{\lambda\mu} = (E_\lambda - E + \Delta_\lambda - i\Gamma_\lambda/2)\delta_{\lambda\mu} \tag{2.62}$$

$$U_{cc'} = e^{-i(\phi_c+\phi_{c'})}\left(\delta_{cc'} + \sum_\lambda \frac{i\sqrt{\Gamma_{\lambda c}\Gamma_{\mu c'}}}{E_\lambda + \Delta_\lambda - E - i\Gamma_\lambda/2}\right) \tag{2.63}$$

2.8.3 The Reich-Moore approximation

In the approximation of Reich and Moore [104] the particularity is used that the amplitudes $\gamma_{\lambda c}$ are uncorrelated and have a Gaussian distribution with zero mean. This is a consequence of the chaotic behaviour of the compound nucleus, except for the very light one. This is known as the Gaussian Orthogonal Ensemble [1, 2, 5].

In medium and heavy nuclei, the number of photon channels is very large. And since the amplitudes are supposed to have a random distribution with zero mean, the expectation value of the product of two amplitudes is zero for $\lambda \neq \mu$, i.e. $< \gamma_{\lambda c}\gamma_{\mu c} >= \gamma_{\lambda c}^2\delta_{\lambda\mu}$. Summing over the photon channels gives

$$\sum_{c\in\text{photon}} \gamma_{\lambda c}\gamma_{\mu c} = \sum_{c\in\text{photon}} \gamma_{\lambda c}^2\delta_{\lambda\mu} = \Gamma_{\lambda\gamma}\delta_{\lambda\mu} \tag{2.64}$$

Therefore the general expression for $\mathbf{A}^{-1}$, equation (2.52), can be simplified for the photon channels and becomes

$$\begin{aligned}\left(\mathbf{A}^{-1}\right)_{\lambda\mu} &= (E_\lambda - E)\delta_{\lambda\mu} - \sum_{c\in\text{photon}} \gamma_{\lambda c}\gamma_{\mu c}(L_c - B_c) - \sum_{c\notin\text{photon}} \gamma_{\lambda c}\gamma_{\mu c}(L_c - B_c) \\ &= (E_\lambda - E)\delta_{\lambda\mu} - \Gamma_{\lambda\gamma}(L_c - B_c)\delta_{\lambda\mu} - \sum_{c\notin\text{photon}} \gamma_{\lambda c}\gamma_{\mu c}(L_c - B_c) \\ &= (E_\lambda - E + \Delta_\lambda - i\Gamma_{\lambda\gamma}/2)\delta_{\lambda\mu} - \sum_{c\notin\text{photon}} \gamma_{\lambda c}\gamma_{\mu c}(L_c - B_c)\end{aligned} \tag{2.65}$$

Comparing this to equation (2.52), the approximation may be written as a reduced R-matrix in the sense that the photon channels are excluded and the eigenvalue E_λ is replaced by $E_\lambda - i\Gamma_{\lambda\gamma}/2$. This Reich-Moore R-matrix is

$$R_{cc'} = \sum_\lambda \frac{\gamma_{\lambda c}\gamma_{\lambda c'}}{E_\lambda - E - i\Gamma_{\lambda\gamma}/2} \qquad c \notin \text{photon} \tag{2.66}$$

Excluding the photon channels, which may be over hundreds of thousands in heavy nuclei, reduces largely the number of channels and therefore the matrix inversion needed in the relation between the R-matrix and the cross sections. In the often occurring case at low energy that only the elastic scattering and neutron capture channels are open, the number of channels in the R-matrix is one, namely that of the neutron channel, the photon channels being excluded explicitly. The total radiation width is present however in the denominator of equation (2.66). The R-matrix becomes in this case an R-function of which the inversion is trivial. Including other channels, like on or two fission channels, keeps the number of channels low and makes the inversion still feasible. This approximation of the general R-matrix is the most accurate one used.

2.9 Average cross sections

With increasing incident neutron energy the widths of the levels become larger than the level spacing and resonances start to overlap. On one hand the level density increases with increasing excitation energy resulting in a smaller level spacing. On the other hand, the average neutron widths increase with energy. The radiation width however is only slowly varying with neutron energy, depending on the number of lower lying levels available for deexcitation of the compound nucleus state. The Doppler broadening of the resonances increases as $\sqrt{E}$. In addition, experimental observations are hindered by resolution broadening, increasing also at higher neutron energies.

At a certain energy, different for each nucleus, the cross sections can not be described by measurable resonance parameters anymore, but can instead be characterized by average parameters, resulting in an average cross section. In this

energy regime, the neutron cross sections can calculated from an approximation by a one-particle potential according to the optical model. The theory developed by Hauser and Feshbach [107–109] relates resonance averaged cross sections for all reaction channels to only few, physical meaningful average parameters, like the neutron and photon strength functions and level densities. In the following only the relevant formulas are given.

The average total cross section $< \sigma_c >$ can, by analogy to equation (2.29), be written as

$$< \sigma_c >= 2\pi \lambda\!\!\!^{-2}_c g_c (1 - \mathrm{Re} < U_{cc} >) \tag{2.67}$$

with the average collision matrix element $< U_{cc} >$ derived from equation (2.45) with $c = c'$. The parameters introduced in a optical model calculation are the penetrabilities or transmission coefficients T_c, corresponding to the formation of the compound nucleus through the channel c.

$$T_c = 1 - | < U_{cc} > |^2 = \frac{4\pi P_c s_c}{|1 - < R_{cc} > (L_c - B_c)|^2} \tag{2.68}$$

with

$$< R_{cc} >= R_c^{\infty} + i\pi s_c \tag{2.69}$$

the channel average R-matrix element with s_c as a quantity proportional to the strength function, and R_c^{∞} a parameter to include the effect of distant levels. The photon and fission transmission coefficients are defined by

$$T_\gamma = 2\pi \frac{< \Gamma_\gamma >}{D_c} \tag{2.70}$$

and

$$T_f = 2\pi \frac{< \Gamma_f >}{D_c} \tag{2.71}$$

The partial reaction cross sections $< \sigma_{cc'} >$ are given by

$$< \sigma_{cc'} >= \pi \lambda\!\!\!^{-2}_c g_c < |\delta_{cc'} - U_{cc'}|^2 > \tag{2.72}$$

which includes the complicated quantity $< |\delta_{cc'} - U_{cc'}|^2 >$ to be calculated with what is known as the GOE triple integral (see also ref. [108] and references therein).

Much progress has been made in the calculation of average cross sections [102]. Measured average cross sections are mostly reported in the evaluated libraries as point-wise data. From these data the level densities and strength functions can be derived. They also serve as a validation of optical model cross section calculations.

Conclusion

Neutron-nucleus reaction data are needed in a wide variety of applications, ranging from parity violation to stellar nucleosynthesis, in addition to the traditional needs from reactor physics. The development of new reactor types or fuel cycles and applications as nuclear waste transmutation has made clear that existing nuclear data are not always of good quality and in some cases are still lacking.

Data are still needed for nuclides to which little attention has been paid in the past since they did not play an important role in conventional reactor safety and criticality calculations. This is the case for nearly all isotopes that are not present or not important in the conventional uranium fuel cycle. Moreover, large deficiencies still exist for difficult cases where samples are radioactive or only available in very small quantities.

The recent renewed interest in nuclear data for new developments in nuclear energy has triggered several activities world-wide. The creation of new, or the refurbishment of existing neutron facilities together with expertise building and data modelling and evaluation activities has contributed to an improved research environment.

References

[1] J. E. Lynn, The Theory of Neutron Resonance Reactions, Clarendon Press, Oxford, 1968.
[2] M. L. Mehta, Nucl. Phys. 18 (1960) 395.
[3] R. U. Haq, A. Pandey, O. Bohigas, Fluctuations properties of nuclear energy levels: Do theory and experiment agree?, Phys. Rev. Lett. 48 (6) (1982) 1086–1089.
[4] O. Bohigas, M. J. Giannoni, C. Schmit, Characterization of chaotic quantum spectra and universality of level fluctuation laws, Phys. Rev. Lett. 52 (1984) 1–4.
[5] M. L. Mehta, Random matrices, academic press Edition, 1991.
[6] C. E. Porter, R. G. Thomas, Fluctuations of nuclear reaction widths, Phys. Rev. 104 (2) (1956) 483–491.
[7] C. Wagemans, The Nuclear Fission Process, CRC, 1991.
[8] A. Gilbert, A. G. W. Cameron, Can. J. Phys. 43 (3) (1965) 1446.
[9] S. F. Mughabghab, M. Divadeenam, N. E. Holden, Neutron cross sections: Neutron resonance parameters and thermal cross sections. Z=1-60, Academic Press, 1981.
[10] S. F. Mughabghab, M. Divadeenam, N. E. Holden, Neutron cross sections: Neutron resonance parameters and thermal cross sections. Z=61-100, Academic Press, 1984.
[11] S. I. Sukhoruchkin, Z. N. Soroko, V. V. Deriglazov, Low Energy Neutron Physics, Volume I/16B, Tables of Neutron Resonance Parameters, Springer, Landolt-Börnstein, 1998.
[12] BROND, russian nuclear data library.
[13] ENDF, ENDF/B-VI, evaluated nuclear data file.
[14] JEFF, Joint european fission and fusion file.
[15] JENDL, Japanese evaluated nuclear data library.
[16] CENDL, Chinese evaluated nuclear data library.
[17] C. S. Wu, et al., Phys. Rev. 105 (1957) 1413.
[18] S. Eidelman, et al., Phys. Lett. B592 (2004) 1.
[19] E. Ambler, et al., Phys. Rev. 106 (1957) 1361.
[20] H. Postma, et al., Physical Review C 24 (1957) 157.
[21] R. P. Feynman, M. Gell-Mann, Phys. Rev. 109 (1958) 193.
[22] E. G. Adelberger, W. C. Haxton, Ann. Rev. Nucl. Part. Sci. 354 (1985) 501.
[23] J. Bendahán, et al., Hyperfine Interactions 34 (1987) 139.
[24] C. Broude, et al., Z. Phys. A336 (1990) 133.
[25] Y. G. Abov, et al., Phys. Lett. 12 (25).

[26] V. P. Alfimenkov, et al., Nuclear Physics A398 (1983) 93.
[27] G. E. Mitchell, J. D. Bowman, H. A. Weidenmüller, Rev. Mod. Phys. 71 (1999) 445.
[28] G. E. Mitchell, J. D. Bowman, S. I. Pentillä, E. I. Sharapov, Phys. Rep. 354 (2001) 157.
[29] J. R. Vanhoy, et al., Z. Phys. A333 (1989) 229.
[30] C. R. Gould, et al. A5 (11) (1990) 2181.
[31] H. Postma, J. D. Bowman, B. E. Crawford, F. Corvi, P. P. J. Delhey, C. M. Frankle, C. A. Grossmann, F. Gunsing, T. Haseyama, J. N. Knudson, L. Y. Lowie, A. Masaike, Y. Matsuda, G. E. Mitchell, S. Penttilä, N. R. Roberson, S. J. Seestrom, E. I. Sharapov, D. A. Smith, S. L. Stephenson, Y. F. Yen, V. W. Yuan, L. Z. (TRIPLE, G. Collaborations), Parity violation at neutron resonances and related neutron spectroscopy experiments, Czech. J. Phys. 51 (2001) A289–A298, suppl. A.
[32] G. S. Mitchell, et al., A measurement of the parity-violating gamma-ray asymmetries in polarized cold neutron capture, Nucl. Instrum. Methods A521 (2004) 468.
[33] F. Gunsing, The spins of resonances in reactions of neutrons with ^{238}U and ^{113}Cd, PhD dissertation, Delft University, iSBN 90-9007923-8 (1995).
[34] F. Gunsing, K. Athanassopulos, F. Corvi, H. Postma, Y. P. Popov, E. I. Sharapov, The spins of resonances in reactions of neutrons with ^{238}U and ^{113}Cd, Physical Review C 56 (3) (1997) 1266–1275.
[35] L. Zanini, F. Corvi, H. Postma, F. Bečvář, Dependence of the populations of low-energy levels in ^{108,110}Ag on the resonance spin and parity, Phys. Rev. C 61 (054616).
[36] Y. Masuda, et al., Parity-violating gamma-ray asymmetry in neutron-proton captur, Nuclear Physics A721 (2003) 485C.
[37] R. A. Alpher, H. A. Bethe, G. Gamow, Phys. Rev. (73) (1948) 803.
[38] E. M. Burbidge, G. R. Burbidge, W. A. Fowler, F. Hoyle, Synthesis of the elements in stars, Rev. Mod. Phys. (29) (1957) 547–650.
[39] G. Wallerstein, et al., Synthesis of the elements in stars: forty years of progress, Rev. Mod. Phys. (69) (1997) 995.
[40] M. Arnould, K. Takahash, Nuclear astrophysics, Rep. Prog. Phys. 62 (1999) 395–464.
[41] A. G. W. Cameron, Pub. Astr. Soc. Pacific (69) (1957) 201.
[42] P. W. Merrill, Science (115) (1952) 484.
[43] nudat, nudata data base, Tech. rep. (2004).
[44] E. Anders, N. Grevesse, Abundances of the elements: Meteoritic and solar, Geochimica et Cosmochimica Acta 53 (1) (1989) 197–214.
[45] F. Gunsing, A. Leprêtre, C. Mounier, C. Raepsaet, C. Bastian, F. Corvi, J. Gonzalez, Stellar neutron capture cross section of ^{99}Tc, Nuclear Physics A688 (2001) 496c–498c.
[46] International Energy Agency, www.iae.org.
[47] Bp statistical review of world energy (2004).

[48] M. Salvatores, I. Slessarev, A. Tchistiakov, The transmutation of long-lived fission products by neutron irradiation, Nucl. Sci. and Eng. 130 (1998) 309–319.
[49] W. Gudowski, Nucl. Phys. A654 (1999) 436c.
[50] S. David, A. Billebaud, M. E. Brandan, R. Brissot, A. Giorni, D. Heuer, J. M. Loiseaux, O. Meplan, H. Nifenecker, J. B. Viano, J. P. Schapira, Fast subcritical hybrid reactors for energy production: evolution of physical parameters and induced radiotoxicities, Nuclear Instruments and Methods in Physics Research Section A: Accelerators, Spectrometers, Detectors and Associated Equipment 443 (2-3) (2000) 510–530.
[51] G. Aliberti, G. Palmiotti, M. Salvatores, C. G. Stenberg, Impact of nuclear data uncertainties on transmutation of actinides in accelerator-driven assemblies, Nucl. Sci. Eng. 146 (1) (2004) 13–50.
[52] A. Bideau, et al., Sensitivity Analysis Of Nuclear Data On k_{eff} For Graphite Moderated Innovative Reactors, OECD/NEA, 2005.
[53] T. R. England, B. F. Rider, Evaluation and compilation of fission product yields, Tech. Rep. LA-UR-94-3106, ENDF-349, LANL (1994).
[54] F. Gunsing, A. Leprêtre, C. Mounier, C. Raepsaet, A. Brusegan, E. Macavero, Neutron resonance spectroscopy of ^{99}Tc from 3 eV to 150 keV, Physical Review C 61 (054608) (2000) 1–13, dAPNIA/SPhN-00-26.
[55] M. Salvatores, A. Zaetta, Les déchets nucléaires, Les Editions de Physique, Paris, 1997.
[56] C. Rubbia, et al., Conceptual design of a fast neutron operated high power energy amplifier, Tech. Rep. CERN/AT/95-44(ET), CERN (1995).
[57] C. D. Bowman, Annu. Rev. Nucl. Part. Sci. 48 (1998) 505.
[58] J. García-Sanz, et al., in: Proc. Int. Conf. Acc. Driven Transm. Techn. Appl. ADTTA, 1999.
[59] C. Rubbia, et al., A realistic plutonium elminiation scheme with fast energy amplifiers and thorium-plutonium fuel, Tech. Rep. CERN/AT/95-53(ET), CERN (1995).
[60] The nea high priority nuclear data request list.
URL `http://www.nea.fr/html/dbdata/hprl/`
[61] B. D. Kuzminov, V. N. Manokhin, in: G. Reffo, A. Ventura, C. Grandi (Eds.), Proc. Int. Conf. Nuclear Data for Science and Technology, 1997, p. 1167.
[62] V. G. Pronyaev, Tech. Rep. INDC(NDS)-408, IAEA (1999).
[63] W. Y. Baek, et al., Nucl. Instr. Meth. B168 (2000) 453.
[64] Y. V. Grigoriev, et al., in: Proc. Int. Sem. Interact. Neutrons with Nuclei, ISINN-8, 2000, p. 68.
[65] G. Lobo, et al., Nucl. Data. Sci. Techn. .
[66] D. Karamanis, et al., Nucl. Sci. and Eng. 139 (2001) 282.
[67] K. Wisshak, F. Voss, F. Käppeler, Nucl. Sci. and Eng. 137 (2001) 183.
[68] P. Schillebeeckx, et al., submitted to Nucl. Sci. and Eng. .
[69] G. Aerts, et al., Measurement of the ^{232}th neutron capture cross section at the CERN n_TOF facility, in: Proc. Int. Conf. Nuclear Data for Science and

Technology, Santa Fe, 2004.
[70] V. McLane, ENDF-102, data formats and procedures for the evaluated nuclear data file ENDF-6, Tech. Rep. BNL-NCS-44945-01, Brookhaven National Laboratory (2001).
[71] Njoy 99, nuclear data processing system (1999).
[72] PREPRO2002: Pre-processing code system for data in ENDF/B format (2002).
[73] U. Agvaanluvsan, G. E. Mitchell, J. F. S. Jr., M. P. Pato, Missing level corrections in nuclear resonances, Nucl. Instr. Meth. A498 (2004) 459–469.
[74] J. M. Salomé, R. Cools, Nucl. Instr. Meth. 179 (1) (1981) 13.
[75] D. Tronc, J. M. Salomé, K. H. Böckhoff, Nucl. Instr. Meth. A228 (1985) 217.
[76] J. M. Salomé, Physicalia 8 (4) (1986) 261.
[77] U. Abbondanno, et al., Neutron capture cross section measurement of ^{151}sm at the CERN neutron time of flight facility (n_TOF), Phys. Rev. Lett. 93 (2004) 161103.
[78] U. Abbondanno, et al., New experimental validation of the pulse height weighting technique for capture cross-section measurements, Nuclear Instruments and Methods in Physics Research Section A: Accelerators, Spectrometers, Detectors and Associated Equipment 521 (2-3) (2004) 454–467.
[79] G. Lorusso, N. Colonna, S. Marrone, G. Tagliente, M. Heil, D. Cano-Ott, M. Mosconi, C. Moreau, A. Mengoni, U. Abbondanno, Time-energy relation of the n_TOF neutron beam: energy standards revisited, Nuclear Instruments and Methods in Physics Research Section A: Accelerators, Spectrometers, Detectors and Associated Equipment 532 (3) (2004) 622–630.
[80] S. Marrone, P. F. Mastinu, U. Abbondanno, R. Baccomi, E. B. Marchi, N. Bustreo, N. Colonna, F. Gramegna, M. Loriggiola, S. Marigo, A low background neutron flux monitor for the n_TOF facility at CERN, Nuclear Instruments and Methods in Physics Research Section A: Accelerators, Spectrometers, Detectors and Associated Equipment 517 (1-3) (2004) 389–398.
[81] C. Borcea, et al., Results from the commissioning of the n_TOF spallation neutron source at CERN, Nucl. Instr. Meth. A513 (2003) 524–537.
[82] C. Borcea, et al., First results from the neutron facility (n_TOF) at CERN, Appl. Phys. A74 (2002) S55–7.
[83] P. M. Milazzo, et al., Measurements of neutron capture cross-sections for ADS-related studies, Nucl. Instr. Meth. B213 (2004) 36–41.
[84] J. L. Tain, F. Gunsing, D. Cano-Ott, N. Colonna, C. Domingo, E. González, M. Heil, F. Käppeler, S. Marrone, P. Mastinu, P. M. Milazzo, T. Papaevangelou, P. Pavlopoulos, R. Plag, R. Reifarth, G. Tagliente, K. Wisshak, Accuracy of the pulse height weighting technique for capture cross section measurements, J. Nucl. Sci. Techn., Sup. 2 (2002) 689–692.
[85] S. Marrone, D. Cano-Ott, N. Colonna, C. Domingo, F. Gramegna, E. M. Gonzalez, F. Gunsing, M. Heil, F. K.appeler, P. F. Mastinu, P. M. Milazzo, T. Papaevangelou, P. Pavlopoulos, R. Plag, R. Reifarth, G. Tagliente, J. L.

Tain, K. Wisshak, Pulse shape analysis of liquid scintillators for neutron studies, Nuclear Instruments and Methods (A490) (2002) 299–307.
[86] W. E. Lamb, Phys. Rev. 55 (1939) 190.
[87] A. Meister, Calculations on lattice vibration effects in the doppler broadening of the 0.18 eV Cd neutron resonance cross section, Tech. Rep. CE/R/VG/78/94, JRC-IRMM (1994).
[88] D. G. Naberejnev, C. Mounier, R. Sanchez, The influence of crystalline binding on resonant absorption and reaction rates, Nucl. Sci. Eng. 131 (1999) 220.
[89] C. Coceva, M. Frisoni, M. Magnani, A. Mengoni, On the figure of merit in neutron time-of-flight measurements, Nucl. Instr. Meth. A489 (2002) 346–356.
[90] E. P. Wigner, L. Eisenbud, Higher angular momenta and long range interaction in resonance reactions, Phys. Rev. 72 (1) (1947) 29–41.
[91] A. M. Lane, R. G. Thomas, R-matrix theory of nuclear reactions, Rev. Mod. Phys. 30 (2) (1958) 257–353.
[92] F. Fröhner, Evaluation and analysis of nuclear resonance data, Tech. Rep. JEFF Report 18, OECD/NEA (2000).
[93] J. Humblet, L. Rosenfeld, Theory of nuclear reactions: I. resonant states and collision matrix, Nucl. Phys. 26 (4) (1961) 529–578.
[94] E. Vogt, Theory of low energy nuclear reactions, Rev. Mod. Phys. 34 (4) (1962) 723–747.
[95] F. Schmittroth, W. Tobocman, Comparison of the *R*-matrix nuclear reaction theories, Phys. Rev. C 3 (1971) 1010–1019.
[96] D. B. Adler, F. T. Adler, Uniqueness of *R*-matrix parameters in the analysis of low-energy neutron cross sections of fissile nuclei, Phys. Rev. C 6 (1972) 986–1001.
[97] C. Chandler, W. Tobocman, *R*-matrix method for nuclear reaction theory, Phys. Rev. C 19 (1979) 1660–1666.
[98] T. A. Brody, J. Flores, J. B. French, P. A. Mello, A. Pandey, S. S. M. Wong, Random-matrix physics: spectrum and strength fluctuations, Rev. Mod. Phys. 53 (1981) 385–479.
[99] J. Humblet, *K*-matrix analysis of resonance nuclear reactions, Phys. Rev. C 42 (4) (1990) 1582–1591.
[100] A. A. Luk'yanov, N. B. Yaneva, Multilevel parametrization of resonance neutron cross sections, Phys. Part. Nucl. 28 (1997) 331–347.
[101] C. R. Brune, Alternative parametrization of *R*-matrix theory, Phys. Rev. C 66 (044611).
[102] E. Bauge, J. P. Delaroche, M. Giro, Lane-consistent, semimicroscopic nucleon-nucleus optical model, Phys. Rev. C 63 (2001) 024607.
[103] J. M. Blatt, L. C. Biedenharn, The angular distribution of scattering and reaction cross sections, Rev. Mod. Phys. 24 (4) (1952) 258–272.
[104] C. W. Reich, M. S. Moore, Multilevel formula for the fission process, Phys. Rev. 111 (3) (1958) 929–933.

[105] P. L. Kapur, R. E. Peierls, Proc. Roy. Soc. A166 (1938) 277.
[106] R. N. Hwang, Nucl. Sci. Eng. 52 (1973) 157.
[107] W. Hauser, H. Feshbach, Phys. Rev. 87 (25) (1952) 366.
[108] F. H. Fröhner, Nucl. Sci. Eng. 103 (1989) 119.
[109] H. Feshbach, Theoretical Nuclear Physics; Nuclear Reactions, John Wiley & Sons, 1991.
[110] F. H. Fröhner, B. Goel, U. Fischer, Fitacs, computer code (1983).
[111] P. M. Koehler, Comparison of white neutron sources for nuclear astrophysics experiments using very small samples, Nucl. Instr. and Meth. A A460 (2001) 352–361.
[112] W. S. Yang, Y. Kim, R. N. Hill, T. A. Taiwo, H. S. Khalil, Nuc. sci. and eng., Long-Lived Fission Product Transmutation Studies 146 (3) (2004) 291–318.
[113] F. Fröhner, Treatment of external levels in neutron resonance fittin: Application to the nonfissile nuclide ^{52}Cr, Nucl. Sci. Eng. 137 (2001) 70–88.
[114] J. Pancin, et al., Measurement of the n_TOF beam profile with a micromegas detector, Nucl. Instr. Meth. A524 (2004) 102–114.
[115] R. Plag, et al., An optimized C_6D_6 detector for studies of resonance-dominated (n,γ) cross-sections, Nucl. Instr. Meth. A496 (2003) 425–436.
[116] M. C. Moxon, J. B. Brisland, REFIT, A least squares fitting program for resonance analysis of neutron transmission and capture data computer code, Tech. rep., United Kingdom Atomic Energy Authority (1991).
[117] J. A. Harvey, Experimental Neutron Resonance Spectroscopy, Academic Press, 1970.
[118] C. Bastian, IEEE Trans. Nucl. Science 43 (4) (1996) 2343.
[119] R. J. M. Konings, J. L. Kloosterman, J. A. Hendriks, H. Gruppelaar, Nucl. Sci. and Eng. 128 (1998) 70.
[120] J. D. Bowman, G. T. Garvey, M. B. Johnson, Annu. Rev. Nucl. Part. Sci. 43 (1993) 829.
[121] A. Stuart, J. K. Ord, Kendall's Advanced Theory of Statistics, Wiley & Sons, 1994.
[122] F. W. Mosteller, J. W. Tukey, Data Analysis and Regression, Addison-Wesly, 1977.
[123] F. Gönnenwein, et al., Nuclear Physics A567 (1994) 303.
[124] F. Käppeler, F. K. Thielemann, M. Wiescher, Current quests in nuclear astrophysics and experimental approaches, Annual Review of Nuclear and Particle Science 48 (1998) 175–251.
[125] S. C. NEA Nuclear Science Committee, Working Party on International Evaluation Co-operation, The NEA high priority nuclear data request list, Tech. rep., OECD-NEA (2001).
[126] F. Käppeler, A. Mengoni, R. Gallino, Neutron capture studies on difficult isotopes - experiments, theory, and astrophysics, Nuclear Physics (A718) (2003) 173c–180c.
[127] F. Bečvář, Simulation of cascades in complex nuclei with emphasis on assessment of uncertainties of cascade-related quantities, Nuclear Instru-

ments and Methods in Physics Research Section A: Accelerators, Spectrometers, Detectors and Associated Equipment 417 (2-3) (1998) 434–449.
[128] F. Kappeler, The origin of the heavy elements: The s process, Progress in Particle and Nuclear Physics 43 (1) (1999) 419–483.
[129] R. L. Macklin, J. H. Gibbons, Neutron capture data at stellar temperatures, Rev. Mod. Phys. 37 (1) (1965) 166–176.
[130] H. R. Weller, N. R. Roberson, Capture reactions with protons, neutrons, and alpha particles, Rev. Mod. Phys. 52 (1980) 699–724.
[131] A. C. Phillips, The physics of stars, John Wiley & Sons, 1994.
[132] D. D. Clayton, Principles of stellar evolution and nucleosynthesis, McGraw-Hill, 1968.
[133] R. Kippenhahn, A. Weigert, Stellar structure and evolution, Springer-Verlag, 1994.
[134] A. G. Sitenko, Theory of Nuclear Reactions, World Scientific, 1990.
[135] B. E. J. Pagel, Nucleosynthesis and Chemical Evolution of Galaxies, Cambridge University Press, 1997.
[136] K. S. Krane, Introductory Nuclear Physics, John Wiley & Sons, 1988.
[137] A. Papoulis, Probability, Random Variables, and Stochastic Processes, McGraw-Hill, 1984.
[138] S. N. Cramer, F. G. Perey, Time-dependent monte carlo calculations of the oak ridge electron linear accelerator target neutron spectrum, NSE 111 (1992) 102–111.
[139] A. J. Ferguson, Angular Correlation Methods in Gamma-Ray Spectroscopy, North-Holland, Amsterdam, 1965.
[140] A. Foderaro, The Elements of Neutron Interaction Theory, Massachusetts Institute of Technology, 1971.
[141] S. Oberstedt, F. Gunsing, γ-decay towards the shape isomeric ground-state of ^{239}U, Nuclear Physics A589 (1995) 435–444.
[142] L. M. Bollinger, G. E. Thomas, p-wave resonances of ^{238}U, Phys. Rev. 171 (4) (1968) 1293–1297.
[143] H. Postma, F. Gunsing, F. Corvi, Improved analysis of parity violation at neutron p-wave resonances of ^{238}U based on resonance spin assignments, Physical Review C 53 (2) (1996) R558–562.
[144] S. Oberstedt, F. Gunsing, Evidence for low-energy γ-decay above the shape isomer in ^{239}U, Nuclear Physics A636 (1998) 129–138.
[145] T. Bolognese, M. Aubert, S. Ayrault, J.-M. Cavedon, F. Chartier, M. Cribier, F. Doneddu, H. Faust, G. Fioni, A. Gaudry, F. Gunsing, F. Lelievre, P. Leconte, F. Marie, J. Martino, R. Oliver, A. Pluquet, M. Spiro, C. Veyssiere, Preliminary results on ^{241}Am transmutation in high thermal flux, Acta Physica Slovaca 49 (1) (1999) 987–994.
[146] G. Fioni, M. Cribier, F. Marie, M. Aubert, S. Ayrault, T. Bolognese, J.-M. Cavedon, F. Chartier, O. Deruelle, F. Doneddu, H. Faust, A. Gaudry, F. Gunsing, P. Leconte, F. Lelievre, J. Martino, R. Oliver, A. Pluquet, S. Rötgger, M. Spiro, C. Veyssiere, Incineration of ^{241}Am induced by thermal neutrons,

Nuclear Physics A693 (2001) 546–564.
[147] F. Corvi, G. Fioni, F. Gunsing, P. Mutti, L. Zanini, Resonance neutron capture in ^{60}Ni below 450 keV, Nuclear Physics A697 (2002) 581–610.

Annex

- Curriculum Vitae
- Liste de publications
- Texte intégral des publications [15,28,38,45,46,66].